

**Kinetic Modeling to Probe the Advanced Oxidation Processes in a
Fe(II)-PAA-ABTS, a Fe(VI)-PAA and a Fe(VI)-Amine Systems**

A Thesis
Presented to
The Academic Faculty

by

Manasa Sadhasivan

In Partial Fulfillment
of the Requirements for the Degree
Master of Science in Environmental Engineering in the
School of Civil and Environmental Engineering

Georgia Institute of Technology
May 2021

COPYRIGHT © 2021 BY MANASA SADHASIVAN

**KINETIC MODELING TO PROBE THE ADVANCED OXIDATION
PROCESSES IN A FE(II)-PAA-ABTS, A FE(VI)-PAA AND A FE(VI)-
AMINE SYSTEMS**

Approved by:

Dr. Ching-Hua Huang, Advisor
School of Civil and Environmental Engineering
Georgia Institute of Technology

Dr. Virender K. Sharma
School of Public Health
Texas A&M University

Dr. Sotira Yiacoumi
School of Civil and Environmental Engineering
Georgia Institute of Technology

Date Approved: [April 30, 2021]

ACKNOWLEDGEMENTS

I would not have successfully completed the thesis without the support and guidance of various people at Georgia Institute of Technology.

Firstly, I would like to express my sincere gratitude to my advisor, Dr. Ching-Hua Huang for her unrelenting support and supervision at every stage of the research project. I would also like to extend my special thanks to Dr. Juhee Kim and Dr. Cong Luo for their contribution, insightful comments and suggestions throughout the past two years. I also appreciate the support from all the members of Dr. Ching-Hua Huang's research group. Lastly, I would like to thank my parents, sister and friends for the constant encouragement throughout this journey.

TABLE OF CONTENTS

ACKNOWLEDGEMENTS	iii
LIST OF FIGURES	vi
SUMMARY	x
CHAPTER 1. Introduction	1
CHAPTER 2. FE(II)-PAA-ABTS SYSTEM	5
2.1 Methodology	5
2.1.1 Chemicals	5
2.1.2 Oxidation of ABTS in Fe(II)-PAA-ABTS System	5
2.1.3 PAA decay in Fe(II)-PAA-ABTS system	6
2.1.4 Kinetic Modelling	7
2.1.5 Sensitivity Analysis and Goodness-of-fit	7
2.2 Results and Discussion	8
2.2.1 Kinetic modelling of ABTS, $ABTS^{\bullet+}$ and PAA at pH 3	11
2.2.2 Sensitivity Analysis and Goodness of Fit	18
2.3 CONCLUSION	21
CHAPTER 3. Fe(VI)-PAA system	23
3.1 Methodology	23
3.1.1 Chemicals	23
3.1.2 Kinetic Modelling	23
3.1.3 Goodness-of-fit	24
3.2 Results and Discussion	24
3.2.1 Kinetic Simulation of Fe(VI) Self-decay	24
3.2.2 Kinetic Simulation of Fe(VI) decay by PAA – Eq. 11	26
3.2.3 Kinetic Simulation of Substrate Degradation (Eq. 12-23)	28
3.2.4 Goodness-of-fit	29
3.3 Conclusion	30
CHAPTER 4. Fe(VI)–DMA system	32
4.1 Methodology	32
4.1.1 Chemicals	32
4.1.2 Kinetic Modeling	32
4.2 Results and Discussion	32
4.3 Conclusion	37
APPENDIX A.	38
Additional Experiments and Kinetic Modelling for the Fe(II)-PAA-ABTS system:	38
REFERENCES	46

LIST OF TABLES

Table 1	Proposed Reactions in the Fe(II)-PAA-ABTS system at	10
Table 2	Sensitivity analysis for the different conditions: $[PAA]_0 = 100 \mu\text{M}$, $[Fe(II)]_0 = 50 \mu\text{M}$, $[ABTS]_0 = 25 \mu\text{M}$, $t = 0-2$ or $0-120$ s	19
Table 3	Goodness of fit test for the Fe(II)-PAA-ABTS system for ABTS and $ABTS_{\bullet}^{+}$ system	20
Table 4	. Goodness of fit test for the Fe(II)-PAA-ABTS system for ABTS and $ABTS_{\bullet}^{+}$ system at $t = 0-120$ s	20
Table 5	Goodness of fit test for the Fe(II)-PAA-ABTS system for PAA system at $t = 0-45$ s	21
Table 6	Proposed Reactions in the Fe(VI)-PAA-substrate system	25
Table 7	Goodness-of-fit test for the Fe(VI)-PAA system for Fe(VI) decay	29
Table 8	Goodness-of-fit test for the Fe(VI)-PAA system for substrate decay	30
Table 9	Proposed reactions for the Fe(VI)-DMA system at pH 9.	33
Table A.1	Sensitivity Coefficients at $[PAA]_0 = 100 \mu\text{M}$, $[Fe(II)]_0 = 50 \mu\text{M}$, $[ABTS]_0 = 25 \mu\text{M}$, $t = 2$ s	40
Table A.2	Sensitivity Coefficients at $[PAA]_0 = 100 \mu\text{M}$, $[Fe(II)]_0 = 50 \mu\text{M}$, $[ABTS]_0 = 25 \mu\text{M}$, $t = 2$ s	42
Table A. 3	Sensitivity Coefficients at $[PAA]_0 = 100 \mu\text{M}$, $[Fe(II)]_0 = 25 \mu\text{M}$, $[ABTS]_0 = 10 \mu\text{M}$, $t = 2$	42
Table A. 4	Sensitivity Coefficients at $[PAA]_0 = 100 \mu\text{M}$, $[Fe(II)]_0 = 25 \mu\text{M}$, $[ABTS]_0 = 10 \mu\text{M}$, $t = 120$ s	43
Table A. 5	Sensitivity Coefficients at $[PAA]_0 = 100 \mu\text{M}$, $[Fe(II)]_0 = 25 \mu\text{M}$, $[ABTS]_0 = 5 \mu\text{M}$, $t = 2$ s	44
Table A. 6	Sensitivity Coefficients at $[PAA]_0 = 100 \mu\text{M}$, $[Fe(II)]_0 = 25 \mu\text{M}$, $[ABTS]_0 = 5 \mu\text{M}$, $t = 120$ s	45

LIST OF FIGURES

- Figure 1 Fe(II)-PAA-ABTS system: Experimental data and kinetic simulation of ABTS and $\text{ABTS}^{\bullet+}$ at A), C), E) 2 s B), D), F) 120s. Solid Symbol: ABTS and $\text{ABTS}^{\bullet+}$ experimental data points. Line: Model Simulation (Experimental Conditions:A) B) $[\text{PAA}]_0 = 100 \mu\text{M}$, $[\text{Fe(II)}]_0 = 50 \mu\text{M}$, $[\text{ABTS}]_0 = 25 \mu\text{M}$, $[\text{H}_2\text{O}_2]_0 = 31 \mu\text{M}$; C) D) $[\text{PAA}]_0 = 100 \mu\text{M}$, $[\text{Fe(II)}]_0 = 25 \mu\text{M}$, $[\text{ABTS}]_0 = 10 \mu\text{M}$, $[\text{H}_2\text{O}_2]_0 = 31 \mu\text{M}$; E) F) $[\text{PAA}]_0 = 100 \mu\text{M}$, $[\text{Fe(II)}]_0 = 25 \mu\text{M}$, $[\text{ABTS}]_0 = 5 \mu\text{M}$, $[\text{H}_2\text{O}_2]_0 = 31 \mu\text{M}$) 12
- Figure 2 Fe(II)-PAA-ABTS system: kinetic simulation of Fe(IV) in reaction conditions, A: $[\text{PAA}]_0 = 100 \mu\text{M}$, $[\text{Fe(II)}]_0 = 50 \mu\text{M}$, $[\text{ABTS}]_0 = 25 \mu\text{M}$; B: $[\text{PAA}]_0 = 100 \mu\text{M}$, $[\text{Fe(II)}]_0 = 25 \mu\text{M}$, $[\text{ABTS}]_0 = 10 \mu\text{M}$; C: $[\text{PAA}]_0 = 100 \mu\text{M}$, $[\text{Fe(II)}]_0 = 25 \mu\text{M}$, $[\text{ABTS}]_0 = 5 \mu\text{M}$. $[\text{H}_2\text{O}_2]_0 = 31 \mu\text{M}$ for all. 14
- Figure 3 Fe(II)-PAA-ABTS system: kinetic simulation of $\text{CH}_3\text{CO}_2^{\bullet}$ in reaction conditions, A: $[\text{PAA}]_0 = 100 \mu\text{M}$, $[\text{Fe(II)}]_0 = 50 \mu\text{M}$, $[\text{ABTS}]_0 = 25 \mu\text{M}$; B: $[\text{PAA}]_0 = 100 \mu\text{M}$, $[\text{Fe(II)}]_0 = 25 \mu\text{M}$, $[\text{ABTS}]_0 = 10 \mu\text{M}$; C: $[\text{PAA}]_0 = 100 \mu\text{M}$, $[\text{Fe(II)}]_0 = 25 \mu\text{M}$, $[\text{ABTS}]_0 = 5 \mu\text{M}$. $[\text{H}_2\text{O}_2]_0 = 31 \mu\text{M}$ for all. 15
- Figure 4 Fe(II)-PAA-ABTS system: kinetic simulation of $\text{CH}_3\text{COOO}^{\bullet}$ in reaction conditions, A: $[\text{PAA}]_0 = 100 \mu\text{M}$, $[\text{Fe(II)}]_0 = 50 \mu\text{M}$, $[\text{ABTS}]_0 = 25 \mu\text{M}$; B: $[\text{PAA}]_0 = 100 \mu\text{M}$, $[\text{Fe(II)}]_0 = 25 \mu\text{M}$, $[\text{ABTS}]_0 = 10 \mu\text{M}$; C: $[\text{PAA}]_0 = 100 \mu\text{M}$, $[\text{Fe(II)}]_0 = 25 \mu\text{M}$, $[\text{ABTS}]_0 = 5 \mu\text{M}$. $[\text{H}_2\text{O}_2]_0 = 31 \mu\text{M}$ for all. 16
- Figure 5 Fe(II)-PAA-ABTS system: Experimental data and kinetic simulation of PAA in reaction conditions, A: $[\text{PAA}]_0 = 100 \mu\text{M}$, $[\text{Fe(II)}]_0 = 50 \mu\text{M}$, $[\text{ABTS}]_0 = 25 \mu\text{M}$, B: $[\text{PAA}]_0 = 100 \mu\text{M}$, $[\text{Fe(II)}]_0 = 25 \mu\text{M}$, $[\text{ABTS}]_0 = 10$, C: $[\text{PAA}]_0 = 100 \mu\text{M}$, $[\text{Fe(II)}]_0 = 25 \mu\text{M}$, $[\text{ABTS}]_0 = 5 \mu\text{M}$. $[\text{H}_2\text{O}_2]_0 = 31 \mu\text{M}$ for all. Solid Symbol: Experimental data. Line: Model Simulation 17
- Figure 6 Fe(II)-PAA-ABTS system: Experimental data and kinetic simulation of ABTS and $\text{ABTS}^{\bullet+}$ at A) $[\text{PAA}]_0 = 100 \mu\text{M}$, $[\text{Fe(II)}]_0 = 25 \mu\text{M}$, $[\text{ABTS}]_0 = 10 \mu\text{M}$ and B) $[\text{PAA}]_0 = 100 \mu\text{M}$, $[\text{Fe(II)}]_0 = 25 \mu\text{M}$, $[\text{ABTS}]_0 = 5 \mu\text{M}$ with and without Eq. 13. 18
- Experimental data and kinetic simulation of Fe(VI) decay in the Fe(VI)-PAA system. Solid symbols: experimental data for Fe(VI) decay. (Experimental conditions: $[\text{Fe(VI)}]_0 = 50.0\text{-}400.0$) 18

	μM , $[\text{PAA}]_0 = 100.0 \mu\text{M}$ (A)(C) and $50.0 \mu\text{M}$ (B)(D), 10.0 mM borate buffer, and $\text{pH} = 9.0$). Line: model simulation.	
Figure 8	Experimental data and kinetic simulation of degradation of substrates in the Fe(VI)-PAA-substrate system. Experimental conditions: $[\text{Fe(VI)}]_0 = 200.0 \mu\text{M}$, $[\text{PAA}]_0 = 100.0 \mu\text{M}$, $[\text{pharmaceutical}]_0 = 10.0 \mu\text{M}$, $\text{pH} = 9.0 \pm 0.1$, 10.0 mM borate buffer, $T = 25 \pm 1 \text{ }^\circ\text{C}$. (A) Antibiotics: SMX-sulfamethoxazole, SDM-sulfadimethoxine, and TMP-trimethoprim. (B) Beta blockers: ATL-atenolol, and PPN-propranolol. Stimulant: CAF-caffeine.	17
Figure 9	Experimental data and kinetic simulation of Fe(VI) decay in the Fe(VI)-DMA system for 5 seconds. Solid symbol: experimental data for Fe(VI) decay by DMA. Experimental conditions: $[\text{DMA}]_0 = 5.0 - 20.0 \text{ mM}$, $[\text{Fe(VI)}]_0 = 50.0 \mu\text{M}$, $\text{pH} = 9.0$, 10.0 mM borate buffer. Line: model simulation.	28
Figure 10	Experimental data and kinetic simulation of degradation of substrates in the Fe(VI)-PAA-substrate system. Experimental conditions: $[\text{Fe(VI)}]_0 = 200.0 \mu\text{M}$, $[\text{PAA}]_0 = 100.0 \mu\text{M}$, $[\text{pharmaceutical}]_0 = 10.0 \mu\text{M}$, $\text{pH} = 9.0 \pm 0.1$, 10.0 mM borate buffer, $T = 25 \pm 1 \text{ }^\circ\text{C}$. (A) Antibiotics: SMX-sulfamethoxazole, SDM-sulfadimethoxine, and TMP-trimethoprim. (B) Beta blockers: ATL-atenolol, and PPN-propranolol. Stimulant: CAF-caffeine.	29
Figure 11	Experimental data and kinetic simulation of Fe(VI) decay in the Fe(VI)-DMA system for 5 seconds. Solid symbol: experimental data for Fe(VI) decay by DMA. Experimental conditions: $[\text{DMA}]_0 = 5.0 - 20.0 \text{ mM}$, $[\text{Fe(VI)}]_0 = 50.0 \mu\text{M}$, $\text{pH} = 9.0$, 10.0 mM borate buffer. Line: model simulation.	34
Figure 12	Experimental data of Fe(VI) decay in the Fe(VI)/DMA system for 30 seconds. (Experimental condition: $[\text{DMA}]_0 = 5.0 - 20.0 \text{ mM}$, $[\text{Fe(VI)}]_0 = 50.0 \mu\text{M}$, $\text{pH} = 9.0$, 10.0 mM borate buffer).	35
Figure A.1	Experimental data and kinetic simulation of ABTS and $\text{ABTS}^{\bullet+}$ at A), C) 120 s B), D) 2s. Solid Symbol: ABTS and $\text{ABTS}^{\bullet+}$ experimental data points. Line: Model Simulation (Experimental Conditions: A) B) $[\text{PAA}]_0 = 50 \mu\text{M}$, $[\text{Fe(II)}]_0 = 50 \mu\text{M}$, $[\text{ABTS}]_0 = 25 \mu\text{M}$, $[\text{H}_2\text{O}_2]_0 = 31 \mu\text{M}$, C) D) $[\text{PAA}]_0 = 25 \mu\text{M}$, $[\text{Fe(II)}]_0 = 50 \mu\text{M}$, $[\text{ABTS}]_0 = 25 \mu\text{M}$, $[\text{H}_2\text{O}_2]_0 = 31 \mu\text{M}$	37
Figure A. 2	Experimental data and kinetic simulation of PAA in reaction conditions, A: $[\text{PAA}]_0 = 100 \mu\text{M}$, $[\text{Fe(II)}]_0 = 75, 60, 50, 40 \mu\text{M}$, $[\text{ABTS}]_0 = 25 \mu\text{M}$, B: $[\text{PAA}]_0 = 75 \mu\text{M}$, $[\text{Fe(II)}]_0 = 75, 60, 50,$	40

40 μM , $[\text{ABTS}]_0 = 25 \mu\text{M}$. $[\text{H}_2\text{O}_2]_0 = 31 \mu\text{M}$ for all. Solid
Symbol: Experimental data. Line: Model Simulation

LIST OF SYMBOLS AND ABBREVIATIONS

AOP = Advanced Oxidation Process

PAA – Peracetic acid

ABTS - 2,2'-azino-bis(3-ethyl-benzothiazoline-6-sulfonic acid)

QFS – Quench flow system

TIC - Thiel's inequality coefficient

NRMSE - Normalized root mean square error

ME - Model efficiency

SUMMARY

Pharmaceuticals are one of the major groups of emerging environmental contaminants in recent years. Advanced oxidation processes (AOPs) are known to be more efficient than conventional treatment processes in the degradation of pharmaceutical micropollutants. Novel AOPs use several oxidants such as ferrate (Fe(VI)) and peracetic acid (PAA) in order to generate highly reactive species which further degrade micropollutants. Furthermore, suitable activators can be combined with the oxidants to produce enhanced efficient in AOPs. The overall objective of this study is to investigate qualitatively and quantitatively the reaction mechanisms of the iron intermediate species (Fe(V) and Fe(IV)) in three different AOP systems that exploit the oxidizing potential of Fe(VI) or activated Fe(II). The three systems investigated are the Fe(II)-PAA-ABTS (2,2'-azino-bis(3-ethyl-benzothiazoline-6-sulfonic acid), Fe(VI)-PAA and Fe(VI)-DMA systems. The experimental results are collected and examined in depth by constructing robust kinetic models for the respective oxidative systems to study the mechanisms involved. Sensitivity analysis and goodness-of-fit tests are further conducted to validate the kinetic models. Overall, this study presents a useful methodology and new modeling tools to quantitatively probe the advanced oxidation systems to gain new insights in the mechanism involved.

CHAPTER 1. INTRODUCTION

Pharmaceuticals, ironical to its known use to cure diseases, are emerging as important environmental contaminants. Major sources include improper disposal into soils and water bodies through unused or human excreted drugs from sectors such as industries, hospitals, and domestic wastes and from agricultural manures and runoffs.¹⁻⁴

Although conventional treatment methods are widely known and applied, they are not as effective as advanced oxidation processes (AOPs) in eliminating the micropollutants of concern in water.⁵⁻⁷ AOPs rely on the generation of highly reactive radicals capable of oxidizing organic contaminants. They use several oxidants to achieve this goal, such as hydrogen peroxide, chlorine, ozone, persulfate, peracetic acid and others.⁸⁻¹¹ In recent years, advanced oxidation technologies based on high-valent iron (e.g., Fe(VI), Fe(V) and Fe(IV)) and peracetic acid (PAA) are becoming of great interest as novel AOPs. This study focuses on the investigation of the mechanisms involved in some of these oxidation systems.¹²

PAA is an emerging oxidant that is gaining research attention lately. PAA is highly advantageous owing to its high antimicrobial activity and lesser formation of harmful disinfection byproducts in comparison to conventional oxidants such as free chlorine.⁴ PAA alone exhibits high selectivity in the reactivity towards organic substrates.¹³ Meanwhile, PAA can be activated in the presence of a suitable promoter, such as light irradiation or metal catalysts, to generate reactive species with high reactivity toward many organic substrates.¹⁴

Utilizing the oxidation potential of PAA in combination with metal ions (e.g., Mn(II/III/IV), Fe(II/III), Co(II/III), Ru(III), and V(VI/V)) has been explored by recent research.^{15-17,18} Although studies are still limited in this area, previous work on AOPs such as the Fenton reaction (Fe(II)/H₂O₂) suggests that Fe(II) could act as an effective activator. Moreover, Fe(II) is easily available and does not cause any harm to the environment. Kim et al. has explored the Fe(II)/PAA AOP and assessed the reactive species that could potentially react with substrates. To improve the fundamental understanding of the

oxidation capacity of the Fe(II)/PAA system, this study introduces 2,2'-azino-bis(3-ethyl-benzothiazoline-6-sulfonic acid) (ABTS) as the substrate of investigation, i.e., a PAA-Fe(II)-ABTS system. The advantage of using ABTS is that ABTS can be easily oxidized to form a relatively stable $\text{ABTS}^{\bullet+}$ radical species that can be measured with high sensitivity using a stopped-flow spectroscopy technique, hence allowing the possibility to quantitatively explore the behavior of reactive species (e.g., oxidized substrate intermediate and Fe(IV)) generation during the very rapid activation and chain reactions of the Fe(II)-PAA advanced oxidation system.

Iron is one of the most widely and easily available metals in the earth's crust. In recent years, ferrate (normally in the form of Fe(VI)) has emerged as a novel oxidant to overcome the drawbacks of other water treatment oxidants, owing to its versatile nature as a chemical oxidant, coagulant and disinfectant. Fe(VI) is considered to be environmentally friendly since it does not form any carcinogenic by-products during oxidation processes. Moreover, activated Fe(VI) systems (i.e., combining Fe(VI) with an activator such as reductants^{19,20} or ions^{21,22,23}) have been explored in recent years which exhibit enhanced efficiency for the degradation of micropollutants. The enhanced efficiency of an activated Fe(VI) system can be attributed to the generation of intermediate Fe(V) and/or Fe(IV) species which are claimed to have at least two orders of magnitude higher reactivity against substrates compared to Fe(VI). The activated Fe(VI) system may exhibit complicated reaction kinetics and generation of several different reactive species that need to be considered for a better understanding of the reaction mechanism.

Recent studies have reported several successful activated Fe(VI) systems, for example activated Fe(VI) by acid, ammonia, sulfite, bicarbonate, Mn(II), and creatinine.^{23,24} However, combining Fe(VI) with PAA (i.e., the Fe(VI)-PAA system) has been studied for the first time by our research lab and collaborators, and it involves the formation of several reactive species (i.e., Fe(IV), $\bullet\text{OH}$, $\text{CH}_3\text{C}(\text{O})\text{O}^\bullet$ and $\text{CH}_3\text{C}(\text{O})\text{OO}^\bullet$) to enhance the degradation efficiency for micropollutants. This study investigates the Fe(VI)-PAA system using kinetic modeling, and specifically evaluates the generation and consumption of the hypothesized Fe(IV) species for substrate degradation. The developed kinetic model is

used to estimate the rate constant of Fe(IV) with a wide range of pharmaceutical micropollutants.

Another avenue to explore is the use of amines as activators to enhance Fe(VI) oxidation (i.e., the Fe(VI)-amine system). Aliphatic amines are prevalent in water bodies due to their extensive use in pharmaceutical, textile and fertilizer industries.²⁴ These amines can potentially cause harm by forming toxic disinfection byproducts when reacting with chlorine in water treatment. Using amine as an activator in the Fe(VI) system helps eliminate amines and other substrates from the environment. The Fe(VI)-amine system produces Fe(V) and/or Fe(IV) as the highly reactive species which could degrade substrates that may be resistant to Fe(VI). This study evaluates the reaction kinetics of the activated Fe(VI) by dimethylamine (DMA) (i.e., the Fe(VI)-DMA system) using a kinetic model to derive mechanistic insights.

The overall objective of this study was to investigate qualitatively and quantitatively the reaction mechanisms of the iron intermediate species (Fe(V) and Fe(IV)) in three different AOP systems that exploit the oxidizing potential of Fe(VI) or activated Fe(II). The three systems considered are:

1. The Fe(II)-PAA-ABTS system
2. The Fe(VI)-PAA system
3. The Fe(VI)-amine system

As detailed in the sections of this thesis, experiments were conducted to study the behaviors of PAA, ABTS, and ABTS^{•+} under various reaction conditions for the Fe(II)-PAA-ABTS system. A stopped-flow spectrophotometer was used to obtain the kinetic trends of ABTS consumption and ABTS^{•+} formation, and a quenched-flow system (QFS) was used to obtain the kinetic trends of PAA decay. The experimental data for the Fe(VI)-PAA system and the Fe(VI)-amine system were provided by our collaborating research lab of Prof. Virender Sharma at Texas A&M University.

For all three reaction systems, suitable kinetic models were proposed and series of experimental results were assessed by the kinetic modeling using SimBiology version 5.7

in MATLAB 2018 to evaluate the significance of the involvement of the concerned species. Sensitivity tests were conducted using an inbuilt MATLAB SimBiology feature to observe the impact of each rate constant on every species considered. The goodness-of-fit was evaluated by computing the Thiel's inequality coefficient (TIC), the normalized root mean square error (NRMSE) and the model efficiency (ME) to assess how well the model predicts the experimentally obtained data. On the basis of the kinetic modeling results, mechanistic insights for the oxidation systems are drawn.

CHAPTER 2. FE(II)-PAA-ABTS SYSTEM

This chapter covers the Fe(II)-PAA-ABTS system. It gives an overview of the chemicals used, experimental data collected, and results and analysis obtained.

2.1 Methodology

2.1.1 Chemicals

2,2'-Azino-bis(3-ethylbenzothiazoline-6-sulfonic acid) (ABTS), peracetic acid (PAA, 32% PAA and <6% H₂O₂ in acetic acid and water), ferrous sulphate (FeSO₄·7H₂O), *N,N*-diethyl-*p*-phenylenediamine (DPD), potassium iodide (KI), KH₂PO₄, and Na₂HPO₄ were purchased from Sigma-Aldrich (St. Louis, MO, USA) or Fisher Scientific (Fair Lawn, NJ, USA). Reagent-grade deionized (DI) water was generated by a Nanopure Millipore (Billerica, MA) water purification system.

2.1.2 Oxidation of ABTS in Fe(II)-PAA-ABTS System

The reaction kinetics in the Fe(II)-PAA-ABTS system were studied by measuring the concentrations of ABTS, ABTS^{•+} and PAA at varied [PAA]₀/[Fe(II)]₀ and [Fe(II)]₀/[ABTS]₀ molar ratios at pH 3.2 ± 0.1. The solution pH was confirmed by measuring the initial and final pHs using a pH meter (Accumet Research AR 20). Freshly prepared ABTS solutions ranging from 5-50 μM and Fe(II) solutions ranging from 25-75 μM were prepared in DI water. PAA solutions ranging from 25-100 μM were also freshly prepared in DI water from the stock solution (50 mM).

The reactions were studied using a stopped-flow spectrophotometer that supported millisecond acquisition rates and was equipped with a UV-vis detector (Olis RSM 1000). The stopped-flow spectrophotometer was operated at scan rates of 1000 scans/sec (0-2 s) and 32 scans/sec (0-120 s). Varied molar ratios of Fe(II), PAA and ABTS were obtained by rapidly mixing a solution of Fe(II) and ABTS with a solution of PAA at equal volumes to initiate the reaction. A mixed solution of Fe(II) and ABTS was prepared just before carrying out the experiments, and it was confirmed that Fe(II) does not react with ABTS.

The consumption of ABTS and the formation of $\text{ABTS}^{\bullet+}$ were determined by monitoring absorbances at 340 nm ($\epsilon_{\text{ABTS}} = 3.66 \times 10^4 \text{ cm}^{-1} \cdot \text{M}^{-1}$) and 415 nm ($\epsilon_{\text{ABTS}^{\bullet+}} = 3.4 \times 10^4 \text{ cm}^{-1} \cdot \text{M}^{-1}$), respectively.²⁵ Note that ABTS does not absorb at 415 nm, and $\text{ABTS}^{\bullet+}$ has absorbance at 340 nm ($\epsilon_{\text{ABTS}^{\bullet+}} = 5.4 \times 10^4 \text{ cm}^{-1} \cdot \text{M}^{-1}$). Concentrations of ABTS and $\text{ABTS}^{\bullet+}$ were calculated based on their measured absorbance and molar absorption coefficients according to the Beer-Lambert law as follows.²²

$$\Delta[\text{ABTS}]_{\text{consumed}} = \frac{\Delta A_{340}}{\epsilon_{\text{ABTS},340} l} - \frac{\epsilon_{\text{ABTS}^{\bullet+},340} \Delta[\text{ABTS}^{\bullet+}]_{\text{formed}}}{\epsilon_{\text{ABTS},340} l} \quad (2.1)$$

$$\Delta[\text{ABTS}^{\bullet+}]_{\text{formed}} = \frac{\Delta A_{415}}{\epsilon_{\text{ABTS}^{\bullet+},415} l} \quad (2.2)$$

where l was the path length and was 2.0 cm at the stopped-flow spectrophotometer.

2.1.3 PAA decay in Fe(II)-PAA-ABTS system

The PAA decay was observed by a customized quenched-flow system (QFS) which was based on previous work.^{4,26,27} The QFS rapidly mixed a solution containing Fe(II) and ABTS with a solution containing PAA, followed by dosing excess of KI, DPD, and phosphate buffer, and analyzed at 515 nm using a UV-Vis spectrophotometer (Beckman DU 520 UV-visible spectrophotometer, Beckman Coulter, Inc., Fullerton, CA). The QFS was set up with three pumps (Harvard Apparatus, South Natick, MA, USA, or KD Scientific Inc., Holliston, MA, USA) and five gas-tight syringes (Hamilton, Reno, NV, USA). The first pump contained two syringes: the first syringe contained a PAA solution and the second syringe contained Fe(II) and ABTS solution. Two solutions were mixed and flowed through different length of loops (PEEK tubing). The lengths were 4.6, 14.5, 36.4, 77.5, and 157.1 cm. This mixture was quenched by excess KI (240 mM) delivered from the second pump. Then, this mixture was mixed with DPD solution and phosphate buffer delivered from the third pump. Each pump was set at a different flow rate ranging from 0.5 to 5.0 mL/min and the reaction time (0.4 - 46 seconds) was obtained with respect to the varied lengths of loops. The solutions from each syringe were rapidly mixed through the mixing tee (VICI Jour Research, Onsala, Sweden) with a dead volume of 25 μL . The absorbance at 515 nm was measured within 60 s after DPD and buffer were finally added

from the third pump. The presence of ABTS^{•+} in a mixed solution resulted in a small contribution of absorbance at 515 nm. The absorbance of ABTS^{•+} was subtracted from that of the mixed solution. After each experiment, the syringes were cleansed with methanol, 0.5 M sulfuric acid in water, and DI water thoroughly before the next experiment.

2.1.4 Kinetic Modeling

The kinetic simulation was conducted using the SimBiology version 5.7 in MATLAB 2018. Initially the Run Scan task in SimBiology was used to predict the rate constant manually followed by using the Fit Data task to narrow down the rate constant using a least-square non-linear regression with constant error model.

2.1.5 Sensitivity Analysis and Goodness-of-fit

The model was validated by computing the Theil's inequality coefficient (TIC),²⁸ the normalized root mean square error (NRMSE)²⁹ and the model efficiency (ME) by following the formulas listed below. The goodness of fit between the experimental and simulated data was compared and quantified.

$$TIC = \frac{\sqrt{\sum_i (y_i - y_{i,m})^2}}{\sqrt{\sum_i y_i^2} + \sqrt{\sum_i y_{i,m}^2}} \quad (2.3)$$

$$NRMSE = \frac{\sqrt{\frac{\sum_i (y_i - y_{i,m})^2}{n}}}{y_{max} - y_{min}} \quad (2.4)$$

$$ME = 1 - \frac{\sum_i (y_i - y_{i,m})^2}{\sum_i (y_i - y_M)^2} \quad (2.5)$$

Where, y_i = Simulated data

$y_{i,m}$ = measured data

y_m = average of simulated data

y_{\max} = maximum of measured data points

y_{\min} = minimum of measured data points

Further, the sensitivity analysis for all the rate constants and its effect on all the concerned species for the different reaction conditions were analyzed using the sensitivity analysis task in Simbiology MATLAB. It was computed for the local sensitivity analysis under the 'Full Normalization' mode. The time dependent sensitivity coefficient was computed based on our previous work.¹² First, it was calculated by

$$\left| \frac{k_j \frac{\partial C_i}{\partial k_j}}{C_i} \right|_t \quad (2.6)$$

To measure the coefficient or impact of one rate constant j on a particular species i, the summation of all the time dependent coefficients were computed as below:

$$\sum_t \left| \frac{k_j \frac{\partial C_i}{\partial k_j}}{C_i} \right|_t \quad (2.7)$$

And to measure the impact of one rate constant j on all the species, the overall sensitivity analysis was calculated by:

$$\sum_i \sum_t \left| \frac{k_j \frac{\partial C_i}{\partial k_j}}{C_i} \right|_t \quad (2.8)$$

where, C_i = Concentration of species i;

k_j = rate constant of reaction j;

t = Time point;

2.2 Results and Discussion

This system at around pH 3 considers the rapid reaction between PAA and Fe(II) to generate Fe(IV) and PAA-related radicals. These reactive species then lose an electron to oxidize ABTS forming $ABTS^{\bullet+}$. $ABTS^{\bullet+}$ is also capable of efficient substrate degradation.

To validate and determine the accurate rate constants, kinetic simulation of the system is carried out by using the equations listed in Table 1.

As shown in Table 1, the reaction between PAA and Fe(II) starts the process and this proceeds in two possible pathways (Eq. 1a, 1b) simultaneously: one forming the acetyloxy radical ($\text{CH}_3\text{CO}_2^\bullet$) and Fe(III) (Eq. 1a), and the second one generating the high valent iron Fe(IV) and acetic acid (Eq. 1b). It should be noted that even though background H_2O_2 ($[\text{H}_2\text{O}_2]_0 = 31 \mu\text{M}$ when $[\text{PAA}]_0 = 100 \mu\text{M}$) coexists with PAA, previous research has shown that PAA reacts with Fe(II) much more rapidly than H_2O_2 .⁴ In other words, PAA dominates the initial reaction kinetics with Fe(II) and thus the reaction of H_2O_2 with Fe(II) was neglected from the model.

After Eq. 1a and 1b, the remaining PAA in the system can react with $\text{CH}_3\text{CO}_2^\bullet$ to form acetylperoxy radical ($\text{CH}_3\text{COOO}^\bullet$) and more acetic acid (Eq. 2). At the same time, $\text{CH}_3\text{CO}_2^\bullet$ and Fe(IV) also undergo decay reactions. $\text{CH}_3\text{CO}_2^\bullet$ undergoes unimolecular decarboxylation to form methyl radical (CH_3^\bullet) (Eq. 6). In the presence of oxygen, CH_3^\bullet quickly reacts with O_2 to form methylperoxy radical ($\text{CH}_3\text{O}_2^\bullet$) which is known to have weak reactivity to organic substrates³⁰ and thus is not considered further in the model. $\text{CH}_3\text{CO}_2^\bullet$ may also be lost from reaction with Fe(II) (Eq. 11). The decay reactions of Fe(IV) involve H_2O_2 (Eq. 7), bimolecular self-decay (Eq. 8), and Fe(II) (Eq. 10). Eq. 13 was proposed for the possible reaction of Fe(IV) with PAA to regenerate Fe(II) and yield acetic acid.

When ABTS is present, the generated Fe(IV) immediately reacts with ABTS to form $\text{ABTS}^{\bullet+}$ and Fe(III) (Eq. 3). ABTS may also react with $\text{CH}_3\text{COOO}^\bullet$ radical (Eq. 5) and $\text{CH}_3\text{CO}_2^\bullet$ radical (Eq. 9) to form $\text{ABTS}^{\bullet+}$ and byproducts, although these reactions appear to be not very significant due to the low concentrations of the radical formation. Eq. 4 represents the reaction of ABTS with Fe(III) generated in the system at a slower rate to yield $\text{ABTS}^{\bullet+}$ and regenerate Fe(II). Eq. 12 is proposed for the reaction of $\text{ABTS}^{\bullet+}$ with Fe(II) to generate Fe(III) and oxidized ABTS (ABTS_{ox}).

The experiments were conducted under different $[\text{PAA}]_0/[\text{Fe(II)}]_0$ and $[\text{Fe(II)}]_0/[\text{ABTS}]_0$ molar ratios. Conceivably, the relative importance of the reactions proposed in Table 1 is

strongly influenced by the molar ratio of $[PAA]_0/[Fe(II)]_0/[ABTS]_0$. When Fe(II) is in excess and PAA is limited, Eq. 10 (decay of Fe(IV) by reacting with Fe(II)) and Eq. 12 (reaction of $ABTS^{\bullet+}$ with Fe(II)) would play a more important role. When $[ABTS]_0$ is lower, excess Fe(IV) would be consumed by undergoing Eq. 13 (reaction of Fe(IV) with PAA), rendering a more important role of this reaction under such conditions.

Table 1 Proposed Reactions in the Fe(II)-PAA-ABTS system at around pH 3.

Reactions	k at pH 3	Reference
[1a] $(Fe^{II})^{2+}(aq) + CH_3CO_3H \rightarrow CH_3CO_2^{\bullet+} + (Fe^{III}OH)^{2+}(aq)$	$7.03 \times 10^4 M^{-1}s^{-1}$	4
[1b] $(Fe^{II})^{2+}(aq) + CH_3CO_3H + 2H_2O \rightarrow H_2Fe^{IV}O_3 + CH_3COOH + 2H^+$	$3.97 \times 10^4 M^{-1}s^{-1}$	4
[2] $CH_3CO_3H + CH_3CO_2^{\bullet} \rightarrow CH_3CO_3^{\bullet} + CH_3COOH$	$(0.01-1) \times 10^7 M^{-1}s^{-1}$	31
[3] $H_2Fe^{IV}O + ABTS + 3H^+ \rightarrow (Fe^{III}OH)^{2+}(aq) + ABTS^{\bullet+} + 2H_2O$	$4.6 \times 10^5 M^{-1}s^{-1}$	12
[4] $(Fe^{III}OH)^{2+}(aq) + ABTS + H^+ \rightarrow (Fe^{II})^{2+}(aq) + ABTS^{\bullet+} + H_2O$	$1.3 \times 10^2 M^{-1}s^{-1}$	32
[5] $CH_3CO_3^{\bullet} + ABTS \rightarrow ABTS^{\bullet+} + CH_3CO_3^-$	$1.8 \times 10^9 M^{-1}s^{-1}$	33
[6] $CH_3CO_2^{\bullet} \rightarrow CH_3^{\bullet} + CO_2$	$2.3 \times 10^5 s^{-1}$	34
[7] $H_2Fe^{IV}O_4 + H_2O_2 + 2H^+ \rightarrow (Fe^{II})^{2+}(aq) + O_2 + 3H_2O$	$1 \times 10^4 M^{-1}s^{-1}$	12
[8] $2 H_2Fe^{IV}O_4 + 4H^+ \rightarrow 2(Fe^{III}OH)^{2+}(aq) + 2H_2O_2$	$1 \times 10^3 M^{-1}s^{-1}$	12
[9] $CH_3CO_2^{\bullet} + ABTS \rightarrow CH_3CO_2^- + ABTS^{\bullet+}$	Less than $1 \times 10^6 M^{-1}s^{-1}$	Estimated in this study

[10] $(\text{Fe}^{\text{II}})^{2+}(\text{aq}) + \text{H}_2\text{Fe}^{\text{IV}}\text{O}_4 \rightarrow 2 (\text{Fe}^{\text{III}}\text{OH})^{2+}(\text{aq}) + \text{O}_2$	$1 \times 10^5 \text{ M}^{-1}\text{s}^{-1}$ $1 \times 10^6 (\text{pH} = 7)$	12
[11] $(\text{Fe}^{\text{II}})^{2+}(\text{aq}) + \text{CH}_3\text{CO}_2^\bullet + \text{H}_2\text{O} \rightarrow (\text{Fe}^{\text{III}}\text{OH})^{2+}(\text{aq}) + \text{CH}_3\text{COOH}$	Less than $1 \times 10^6 \text{ M}^{-1}\text{s}^{-1}$	Estimated in this study
[12] $(\text{Fe}^{\text{II}})^{2+}(\text{aq}) + \text{ABTS}^{\bullet+} + \text{OH}^- \rightarrow (\text{Fe}^{\text{III}}\text{OH})^{2+}(\text{aq}) + \text{ABTS}_{\text{ox}}$	$500 \text{ M}^{-1}\text{s}^{-1}$	Estimated in this study
[13] $\text{H}_2\text{Fe}^{\text{IV}}\text{O}_4 + \text{CH}_3\text{CO}_3\text{H} \rightarrow (\text{Fe}^{\text{II}})^{2+}(\text{aq}) + \text{H}_2\text{O} + 2\text{O}_2 + \text{CH}_3\text{COOH}$	$5 \times 10^4 \text{ M}^{-1}\text{s}^{-1}$	Estimated in this study

2.2.1 Kinetic modeling of ABTS, $\text{ABTS}^{\bullet+}$ and PAA at pH 3

To accurately represent the possible reactions taking place in the Fe(II)-PAA-ABTS system, the equations explained in the previous sections were carefully examined through experimental and kinetic modeling results. The trends of ABTS, $\text{ABTS}^{\bullet+}$ and PAA were monitored and are explained in the sections to come. The conditions considered in this study always contained PAA in excess of Fe(II) and ABTS, and Fe(II) in excess of ABTS, i.e., $[\text{PAA}]_0 > [\text{Fe}(\text{II})]_0 > [\text{ABTS}]_0$. The following three conditions are considered:

- A. $[\text{PAA}]_0 = 100 \mu\text{M}$, $[\text{Fe}(\text{II})]_0 = 50 \mu\text{M}$, $[\text{ABTS}]_0 = 25 \mu\text{M}$
- B. $[\text{PAA}]_0 = 100 \mu\text{M}$, $[\text{Fe}(\text{II})]_0 = 25 \mu\text{M}$, $[\text{ABTS}]_0 = 10 \mu\text{M}$
- C. $[\text{PAA}]_0 = 100 \mu\text{M}$, $[\text{Fe}(\text{II})]_0 = 25 \mu\text{M}$, $[\text{ABTS}]_0 = 5 \mu\text{M}$

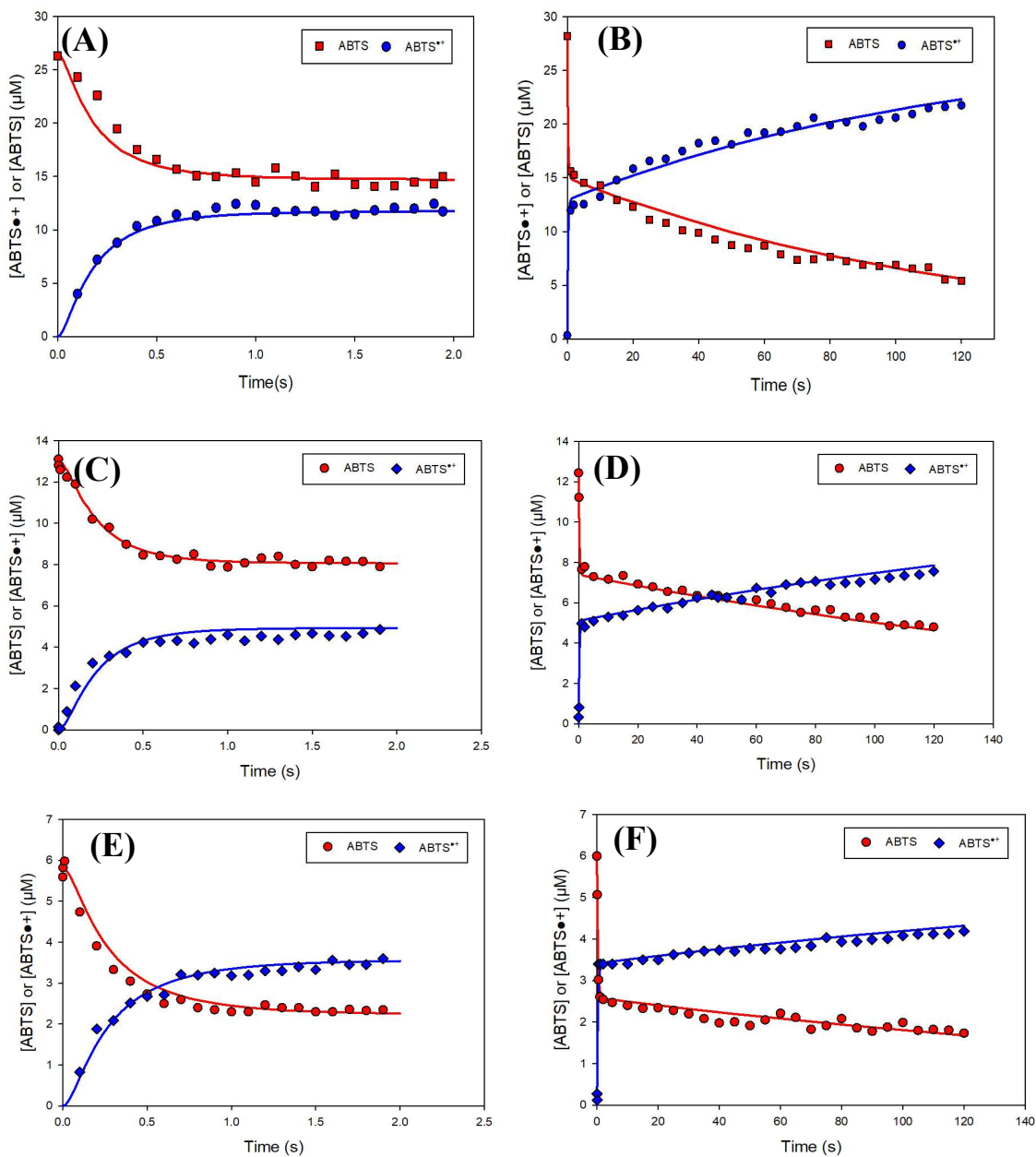


Figure 1. Fe(II)-PAA-ABTS system: Experimental data and kinetic simulation of ABTS and ABTS^{•+} at A), C), E) 2 s B), D), F) 120s. Solid Symbol: ABTS and ABTS^{•+} experimental data points. Line: Model Simulation (Experimental Conditions: A) B) $[\text{PAA}]_0 = 100 \mu\text{M}$, $[\text{Fe(II)}]_0 = 50 \mu\text{M}$, $[\text{ABTS}]_0 = 25 \mu\text{M}$, $[\text{H}_2\text{O}_2]_0 = 31 \mu\text{M}$; C) D) $[\text{PAA}]_0 = 100 \mu\text{M}$, $[\text{Fe(II)}]_0 = 25 \mu\text{M}$, $[\text{ABTS}]_0 = 10 \mu\text{M}$, $[\text{H}_2\text{O}_2]_0 = 31 \mu\text{M}$; E) F) $[\text{PAA}]_0 = 100 \mu\text{M}$, $[\text{Fe(II)}]_0 = 25 \mu\text{M}$, $[\text{ABTS}]_0 = 5 \mu\text{M}$, $[\text{H}_2\text{O}_2]_0 = 31 \mu\text{M}$)

By creating a condition where Fe(II) was completely consumed within the first 2 s by PAA, Fe(III) and Fe(IV) are formed through Eqs. 1a and 1b. But looking at the trends of ABTS from Figure 1, it comes to our notice that ABTS is not fully consumed even though the reactive species formed by PAA and Fe(II) immediately react with ABTS to generate $\text{ABTS}^{\bullet+}$. This makes it clear that there are other competing/scavenging reactions for Fe(IV), $\text{CH}_3\text{COOO}^\bullet$ and $\text{CH}_3\text{CO}_2^\bullet$. But by looking at the profiles of these species through modeling, the amount of $\text{CH}_3\text{COOO}^\bullet$ and $\text{CH}_3\text{CO}_2^\bullet$ formed is 6 orders of magnitude lower than that of Fe(IV) as shown in Figures 2-4. Hence, we can positively infer that Fe(IV) is the major reactive species in this system and other competing reactions involving Fe(IV) affects the consumption and formation of ABTS and $\text{ABTS}^{\bullet+}$. Meanwhile, the low concentration of the radicals can be explained from a close examination of the involved rate constants. The self-decomposition of $\text{CH}_3\text{CO}_2^\bullet$ occurs at a very rapid rate (Eq. 6), and the formation $\text{CH}_3\text{COOO}^\bullet$ depends on the availability of $\text{CH}_3\text{CO}_2^\bullet$ (Eq. 2). The decomposition of the radiacals hinders their reactions with ABTS.

The Fe(IV) profile (Figure 2) suggests that it contributes to the initial spike in the $\text{ABTS}^{\bullet+}$ generation in the 2 second time range, and the later slower increase/decrease in $\text{ABTS}^{\bullet+}$ /ABTS is because of Eq. 4, i.e., the reaction of Fe(III) with ABTS. This reaction is at a comparatively much slower rate and Fe(III) concentration increases once Fe(IV) reacts with all of ABTS.

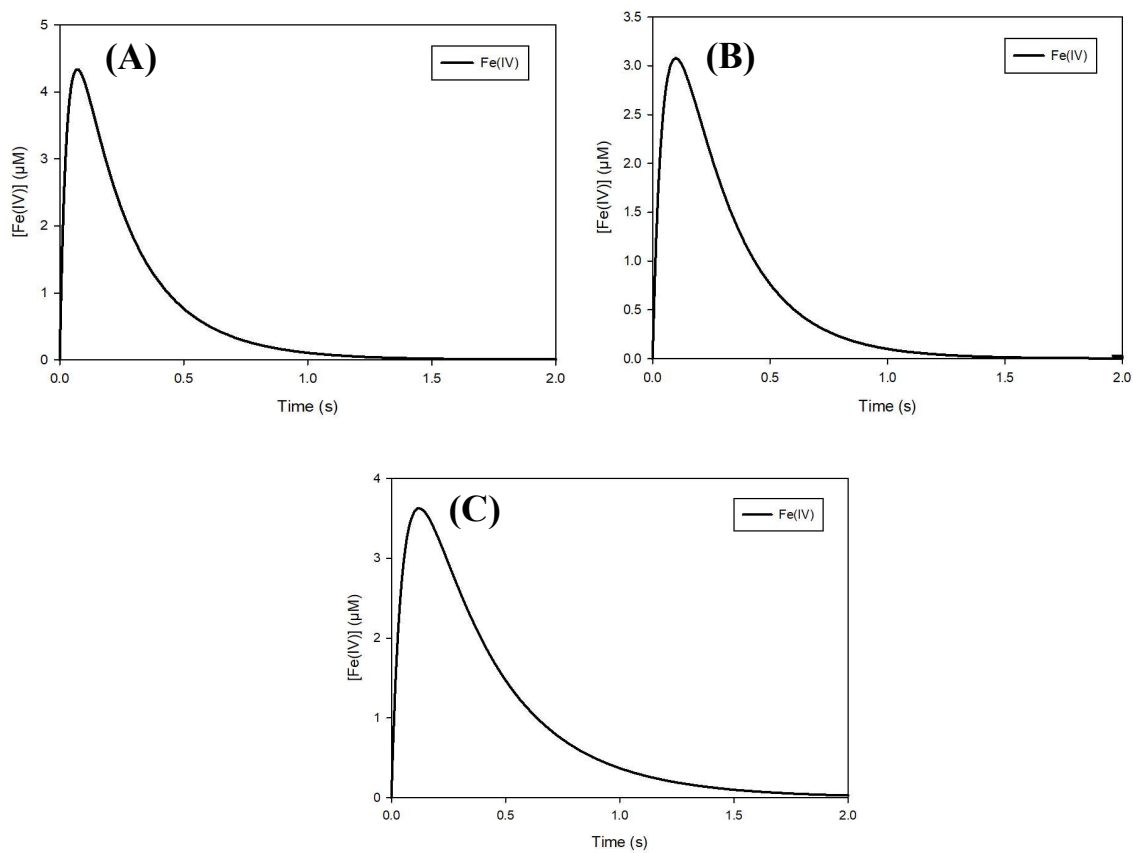


Figure 2. Fe(II)-PAA-ABTS system: kinetic simulation of Fe(IV) in reaction conditions, A: $[\text{PAA}]_0 = 100 \mu\text{M}$, $[\text{Fe(II)}]_0 = 50 \mu\text{M}$, $[\text{ABTS}]_0 = 25 \mu\text{M}$; B: $[\text{PAA}]_0 = 100 \mu\text{M}$, $[\text{Fe(II)}]_0 = 25 \mu\text{M}$, $[\text{ABTS}]_0 = 10 \mu\text{M}$; C: $[\text{PAA}]_0 = 100 \mu\text{M}$, $[\text{Fe(II)}]_0 = 25 \mu\text{M}$, $[\text{ABTS}]_0 = 5 \mu\text{M}$. $[\text{H}_2\text{O}_2]_0 = 31 \mu\text{M}$ for all.

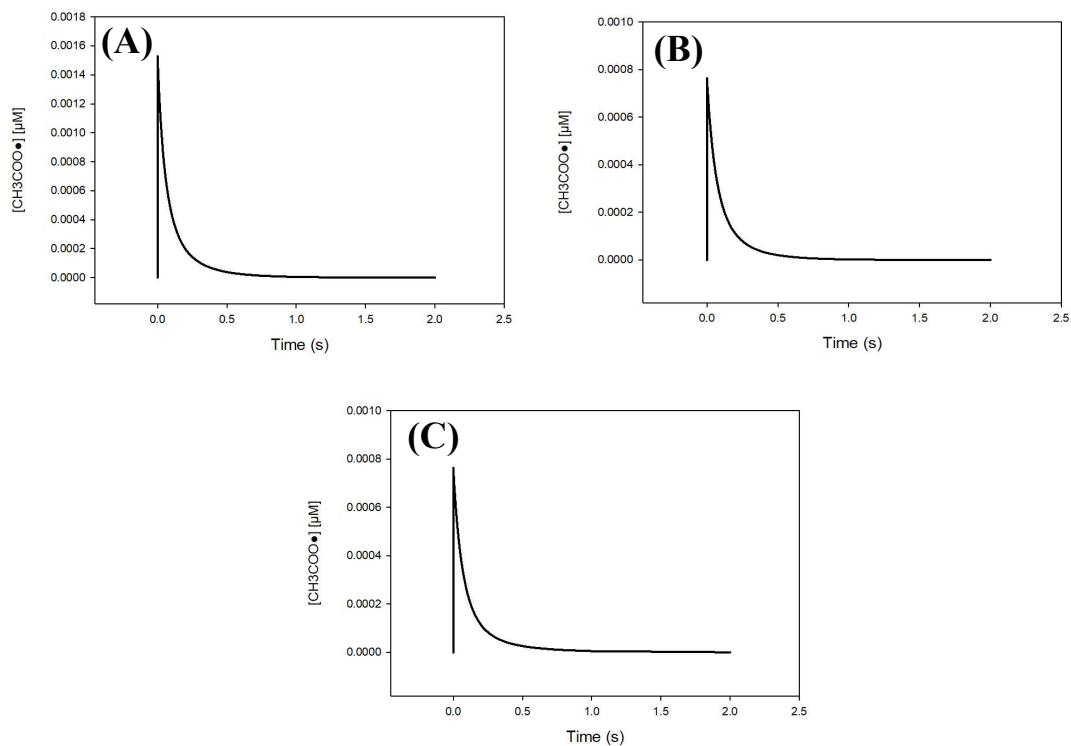
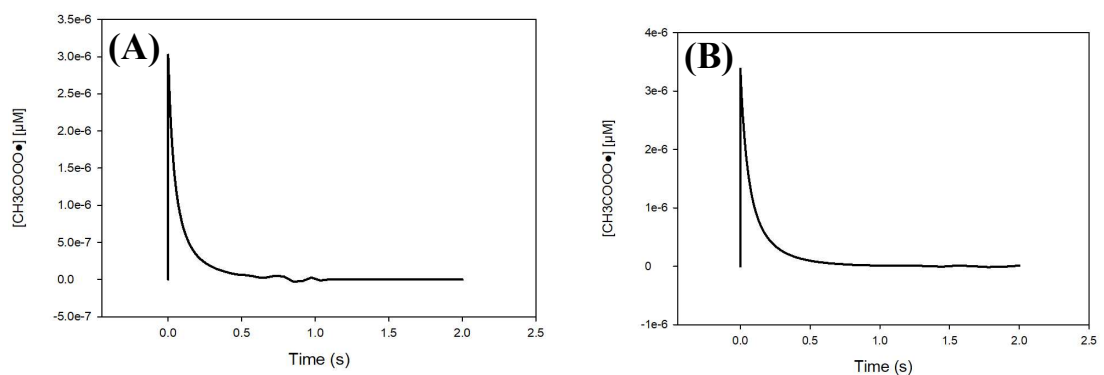


Figure 3. Fe(II)-PAA-ABTS system: kinetic simulation of $\text{CH}_3\text{CO}_2\cdot$ in reaction conditions, A: $[\text{PAA}]_0 = 100 \mu\text{M}$, $[\text{Fe(II)}]_0 = 50 \mu\text{M}$, $[\text{ABTS}]_0 = 25 \mu\text{M}$; B: $[\text{PAA}]_0 = 100 \mu\text{M}$, $[\text{Fe(II)}]_0 = 25 \mu\text{M}$, $[\text{ABTS}]_0 = 10 \mu\text{M}$; C: $[\text{PAA}]_0 = 100 \mu\text{M}$, $[\text{Fe(II)}]_0 = 25 \mu\text{M}$, $[\text{ABTS}]_0 = 5 \mu\text{M}$. $[\text{H}_2\text{O}_2]_0 = 31 \mu\text{M}$ for all.



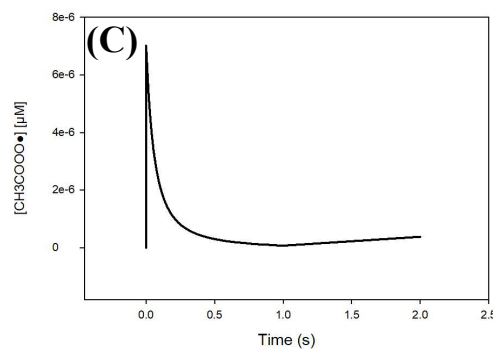
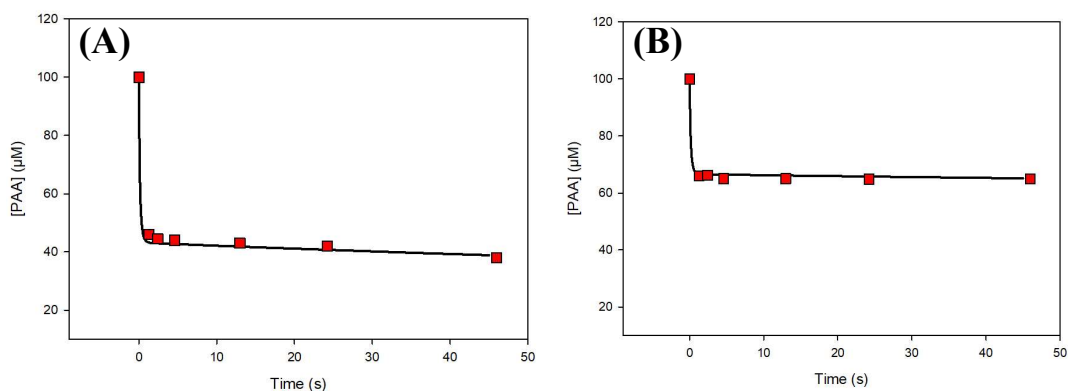


Figure 4. Fe(II)-PAA-ABTS system: kinetic simulation of $\text{CH}_3\text{COOO}^\bullet$ in reaction conditions, A: $[\text{PAA}]_0 = 100 \mu\text{M}$, $[\text{Fe(II)}]_0 = 50 \mu\text{M}$, $[\text{ABTS}]_0 = 25 \mu\text{M}$; B: $[\text{PAA}]_0 = 100 \mu\text{M}$, $[\text{Fe(II)}]_0 = 25 \mu\text{M}$, $[\text{ABTS}]_0 = 10 \mu\text{M}$; C: $[\text{PAA}]_0 = 100 \mu\text{M}$, $[\text{Fe(II)}]_0 = 25 \mu\text{M}$, $[\text{ABTS}]_0 = 5 \mu\text{M}$. $[\text{H}_2\text{O}_2]_0 = 31 \mu\text{M}$ for all.

As shown in Figure 5, the experimental data of PAA decay suggest that no further spontaneous reaction takes place involving PAA, since after the initial decrease within 1.2 s, there is a very slow decay of PAA in most cases. The kinetic simulation well captured the PAA decay trends. These results also support the above inference that Fe(IV) is the major reactive species in reacting with ABTS to produce $\text{ABTS}^{\bullet+}$.



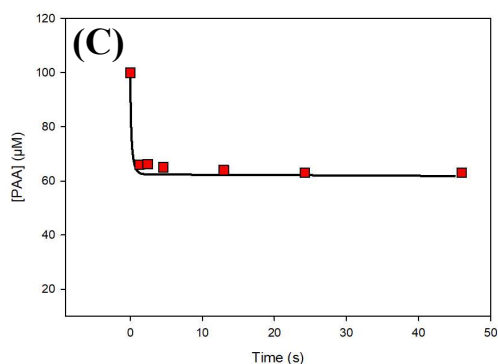


Figure 5. Fe(II)-PAA-ABTS system: Experimental data and kinetic simulation of PAA in reaction conditions, A: $[PAA]_o = 100 \mu\text{M}$, $[Fe(II)]_o = 50 \mu\text{M}$, $[ABTS]_o = 25 \mu\text{M}$, B: $[PAA]_o = 100 \mu\text{M}$, $[Fe(II)]_o = 25 \mu\text{M}$, $[ABTS]_o = 10$, C: $[PAA]_o = 100 \mu\text{M}$, $[Fe(II)]_o = 25 \mu\text{M}$, $[ABTS]_o = 5 \mu\text{M}$. $[H_2O_2]_o = 31 \mu\text{M}$ for all. Solid Symbol: Experimental data. Line: Model Simulation

The two reactions considered in the kinetic model to account for the competing reactions for Fe(IV) in addition to its self-decay reactions are Eq. 10 and 13. Eq. 10, accounts for the excess Fe(II) if any in the system reacting with Fe(IV) to generate more Fe(III). On the other hand, Eq. 13 considers the reaction between PAA and Fe(IV), particularly when there is excess PAA and a low ABTS concentration. As shown in Figure 6, in the conditions when $[ABTS]_o$ is low (much lower than $[Fe(II)]_o$), the competition of PAA with ABTS in reacting with Fe(IV), as accounted by Eq. 13, is important to properly depict the decay trends of ABTS degradation and $ABTS^{\bullet+}$ formation.

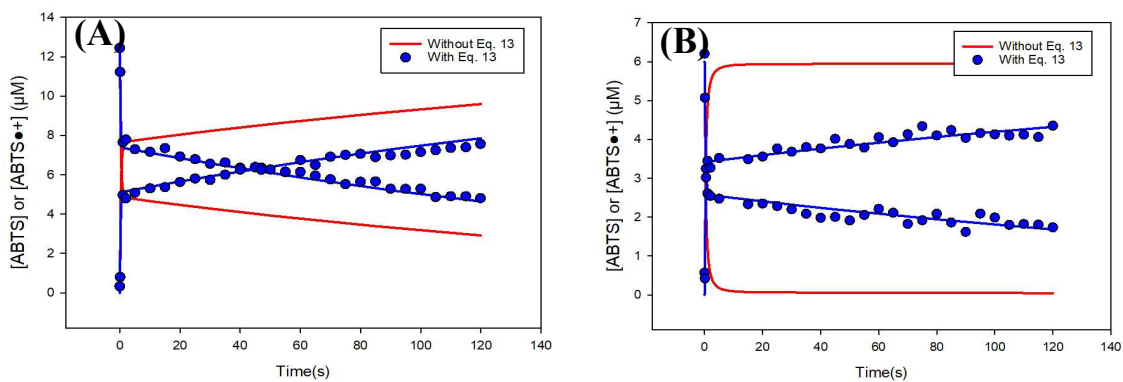


Figure 6. Fe(II)-PAA-ABTS system: Experimental data and kinetic simulation of ABTS and $\text{ABTS}^{\bullet+}$ at A) $[\text{PAA}]_0 = 100 \mu\text{M}$, $[\text{Fe(II)}]_0 = 25 \mu\text{M}$, $[\text{ABTS}]_0 = 10 \mu\text{M}$ and B) $[\text{PAA}]_0 = 100 \mu\text{M}$, $[\text{Fe(II)}]_0 = 25 \mu\text{M}$, $[\text{ABTS}]_0 = 5 \mu\text{M}$ with and without Eq. 13.

2.2.2 Sensitivity Analysis and Goodness of Fit

To evaluate the importance of the Eqs. 1 – 13 in Table 1 for the major species of interest (i.e., ABTS, $\text{ABTS}^{\bullet+}$, PAA, Fe(II), Fe(IV), $\text{CH}_3\text{CO}_2^{\bullet}$, $\text{CH}_3\text{COOO}^{\bullet}$ and Fe(III)) in the Fe(II)-PAA-ABTS system, the local sensitivity analysis was carried out as mentioned in the methodology section. The rankings of the reactions for their impacts are shown in Table 2. The calculated sensitivity coefficients can be found in Appendix A. The higher the sensitivity coefficient, the more dominant the rate constant in the evolution of the species in consideration.

Table 2 depicts the rankings of the impact each rate constant has in the overall reaction under different reaction conditions. The three different sets of reaction conditions at two different time ranges (0-2 s and 0-120 s) are compared and the overall sensitivity was reported in Table 2. We can see that at Condition A: $[\text{PAA}]_0 = 100 \mu\text{M}$, $[\text{Fe(II)}]_0 = 50 \mu\text{M}$, $[\text{ABTS}]_0 = 25 \mu\text{M}$, k_{1a} , k_{1b} , k_4 , k_2 , k_3 , k_6 and k_5 are the most significant ones for both time ranges combined. This shows that at this condition, with ABTS concentration higher, the competing reactions for Fe(IV) (i.e., Eqs. 10 and 13) are not impactful, rather the initial reactions contribute towards the generation of $\text{ABTS}^{\bullet+}$. As we move to a condition with a much lower ABTS concentration (i.e. Conditions B and C when $[\text{ABTS}]_0 = 10$ and $5 \mu\text{M}$, respectively), in addition to the above mentioned rate constants, k_{10} and k_{13} also become sensitive. This indicates the importance of including Eq. 10 and Eq. 13 in the model. Figure 6 above provides a visual depiction of the significance of Eq. 13 and supports the addition of this reaction.

Another thing to note is that k_2 (reaction of $\text{CH}_3\text{CO}_2^{\bullet}$ with PAA to form $\text{CH}_3\text{COOO}^{\bullet}$) was highly sensitive in the 2 s region but was not very important in the 120 s region, which adds to Figures 3 and 4 and supports that the PAA radicals are not significant contributors to the $\text{ABTS}^{\bullet+}$ generation.

Table 2. Sensitivity analysis for the different conditions: [PAA]_o = 100 μM, [Fe(II)]_o = 50 μM, [ABTS]_o = 25 μM, t = 0-2 or 0-120 s.

Reaction condition	Time	Sensitivity Coefficient	The Rank of Sensitivity Coefficient
[PAA] _o = 100 μM, [Fe(II)] _o = 50 μM, [ABTS] _o = 25 μM	2	Overall	$k_{1a} > k_{1b} > k_2 > k_3 > k_6 > k_{13} > k_{10} > k_5 >$ $k_{12} > k_4 > k_{11} > k_7 > k_9 > k_8$
	120		$k_4 > k_5 > k_3 > k_{1b} > k_{1a} > k_{13} > k_6 > k_9 >$ $k_{10} > k_{12} > k_2 > k_{11} > k_7 > k_8$
[PAA] _o = 100 μM, [Fe(II)] _o = 25 μM, [ABTS] _o = 10 μM	2	Overall	$k_{1a} > k_{1b} > k_3 > k_6 > k_{13} > k_2 > k_5 >$ $k_{10} > k_4 > k_7 > k_8 > k_{12} > k_{11} > k_9$
	120		$k_{11} > k_4 > k_9 > k_{1b} > k_5 > k_{1a} > k_{10} >$ $k_3 > k_{13} > k_8 > k_6 > k_2 > k_{12} > k_7$
[PAA] _o = 100 μM, [Fe(II)] _o = 25 μM, [ABTS] _o = 5 μM	2	Overall	$k_{1a} > k_6 > k_{1b} > k_2 > k_4 > k_8 > k_3 > k_5 >$ $k_{13} > k_7 > k_9 > k_{11} > k_{12} > k_{10}$
	120		$k_8 > k_{1a} > k_{10} > k_{1b} > k_3 > k_5 > k_{13} >$ $k_7 > k_2 > k_{12} > k_{11} > k_6 > k_9$

As reported in Tables 3-5, the TIC, NRMSE and ME for all the conditions considered were well within the range expected for good agreement between the experimental and simulated data sets. According to previous studies a value of TIC lower than $0.3^{28,29,35}$ and a $ME^{29,36}$ around 1 indicate a good fit of the two sets of data under consideration.

Table 3. Goodness of fit test for the Fe(II)-PAA-ABTS system for ABTS and $ABTS^{\bullet+}$ system at $t = 0-2$ s

Condition	Time (s)	Species	TIC	NRSME	ME
[PAA] _o = 100 μM, [Fe(II)] _o = 50 μM, [ABTS] _o = 25 μM	2	ABTS	3.3×10^{-2}	8.0×10^{-2}	0.86
		$ABTS^{\bullet+}$	4.3×10^{-2}	7.1×10^{-2}	0.89
[PAA] _o = 100 μM, [Fe(II)] _o = 25 μM, [ABTS] _o = 10 μM	2	ABTS	3.6×10^{-2}	1.5×10^{-1}	0.85
		$ABTS^{\bullet+}$	1.7×10^{-1}	2.7×10^{-1}	0.55
[PAA] _o = 100 μM, [Fe(II)] _o = 25 μM, [ABTS] _o = 10 μM	2	ABTS	3.7×10^{-2}	6.6×10^{-2}	0.96
		$ABTS^{\bullet+}$	7.1×10^{-2}	1.0×10^{-1}	0.91

Table 4. Goodness of fit test for the Fe(II)-PAA-ABTS system for ABTS and $ABTS^{\bullet+}$ system at $t = 0-120$ s

Condition	Time (s)	Species	TIC	NRSME	ME
[PAA] _o = 100 μM, [Fe(II)] _o = 50 μM, [ABTS] _o = 25 μM	120	ABTS	7.6×10^{-2}	8.0×10^{-2}	0.86
		$ABTS^{\bullet+}$	4.7×10^{-2}	7.1×10^{-2}	0.91
	120	ABTS	4.5×10^{-2}	1.0×10^{-1}	0.93

[PAA] _o = 100 μM, [Fe(II)] _o = 25 μM, [ABTS] _o = 10 μM		ABTS ^{•+}	6.0×10^{-2}	9.9×10^{-2}	0.89
[PAA] _o = 100 μM, [Fe(II)] _o = 25 μM, [ABTS] _o = 10 μM	120	ABTS	7.3×10^{-2}	1.1×10^{-1}	0.84
		ABTS ^{•+}	3.9×10^{-2}	7.1×10^{-2}	0.94

Table 5. Goodness of fit test for the Fe(II)-PAA-ABTS system for PAA system at t = 0-45 s

Condition	Time (s)	Species	TIC	NRSME	ME
[PAA] _o = 100 μM, [Fe(II)] _o = 50 μM, [ABTS] _o = 25 μM	45	PAA	1.0×10^{-2}	2.0×10^{-2}	0.99
[PAA] _o = 100 μM, [Fe(II)] _o = 25 μM, [ABTS] _o = 10 μM	45	PAA	1.1×10^{-2}	4.1×10^{-2}	0.98
[PAA] _o = 100 μM, [Fe(II)] _o = 25 μM, [ABTS] _o = 10 μM	45	PAA	1.6×10^{-2}	6.5×10^{-2}	0.96

2.3 CONCLUSION

This study was an effort to improve the mechanistic understanding of reactive species generation in the reaction of PAA with Fe(II) by including ABTS as the substrate. A robust kinetic model was developed for the Fe(II)-PAA-ABTS system to investigate the mechanisms involved and to delineate the major reaction pathways of the system. The

contribution and reactions involving the Fe(IV) reactive intermediate are found to be most influential and have been the major focus of this study. The proposed kinetic model is well supported by a good amount of experimental data and other validation simulation experiments. Future research should be conducted with more experiments at different conditions of $[PAA]_0/[Fe(II)]_0$ ratios in order to more comprehensively test the robustness of this kinetic model, which will improve its suitability for a wider range of reaction conditions and probe further mechanistic insight.

CHAPTER 3. FE(VI)-PAA SYSTEM

3.1 Methodology

3.1.1 Chemicals

Potassium ferrate(VI) (K_2FeO_4) was prepared at Dr. Virender Sharma's laboratory at Texas A&M University (TAMU). Carbamazepine (CBZ), sulfamethoxazole (SMX, purity > 98%), sulfadimethoxine sodium (SDM, analytical standard), trimethoprim (TMP, purity > 98.0%), atenolol (ATL, purity \geq 98%), propranolol hydrochloride (PPN, purity \geq 97%), and caffeine (CAF, ReagentPlus) were purchased from Fisher-Scientific (Austin, TX, USA) or Sigma-Aldrich (St. Louis, MO, USA). A 35% PAA solution (35.5% PAA, 6.5% H_2O_2 and 40% acetic acid in water) was obtained from Pfaltz & Bauer (Waterbury, CT, USA). They followed a wet chemical method³⁷ to synthesize solid potassium ferrate (VI) with a purity >95%. All solutions were prepared using ultrapure water (18.0 M Ω -cm Milli-Q water purification system) (Millipore, Waters Alliance, Milford, MA, USA). All experiments were performed in 0.01 M borate buffer at pH 9.0 ± 0.1 by collaborators at the Texas A&M university.

3.1.2 Kinetic Modeling

The experimental data for the Fe(VI)-PAA system and the Fe(VI)-PAA-substrate system were obtained at various reaction ratios of $[PAA]_0$ and $[Fe(VI)]_0$ from Dr. Sharma's group at the Texas A&M University. $[PAA]_0$ ranged from 50-100 μ M and $[Fe(VI)]_0$ ranged from 50-400 μ M. This report investigates the kinetic modeling of the Fe(VI)-PAA system with and without substrates to delineate the reaction mechanisms involved. The modeling involves two parts:

- A) Modeling the Fe(VI) decay in the Fe(VI)-PAA system

B) Modeling the substrate decay in the Fe(VI)-PAA-substrate system

3.1.3 Goodness-of-fit

The model was validated by quantifying the goodness-of-fit by computing the Theil's inequality coefficient (TIC)²⁸, the normalized root mean square error (NRMSE)²⁹ and the model efficiency (ME) by following the method mentioned in Chapter 2.

3.2 Results and Discussion

Kinetic simulations of Fe(VI) decay in the Fe(VI)-PAA system and substrate degradation in the Fe(VI)-PAA-substrate system were conducted using the experimental data from Dr. Sharma's group. Based on the fitting results, the major reactive species and the rate constants of substrate degradation were proposed. Table 4 presents the proposed reactions in the Fe(VI)-PAA-substrate system. The self-decay and scavenging reactions of Fe(VI), Fe(V), and Fe(IV) were considered in Eqs. 1-10. Then, the reaction of Fe(VI) with PAA to produce Fe(IV) as the major reactive species (Eq. 11) was proposed to be the most significant reaction, and hence this reaction has been explored to fit the Fe(VI) decay data. Eqs. 12-23 were included to study the substrate degradation by Fe(IV) and Fe(VI) in the Fe(VI)-PAA-substrate system, for several pharmaceutical micropollutants: sulfamethoxazole (SMX), sulfadimethoxine (SDM), trimethoprim (TMP), atenolol (ATL), propranolol (PPN) and caffeine (CAF).

3.2.1 Kinetic Simulation of Fe(VI) Self-decay

Eqs. 1-10 in this model include the Fe(VI) self-decay system as described at pH 9.0. Eq. 1 is the starting reaction where one molecule of Fe(VI) undergoes self-decay to form one molecule of Fe(IV) and H₂O₂. The Fe(VI) now reacts with the H₂O₂ (Eq. 2) in the system to further generate more Fe(IV) and releases one molecule of oxygen. The Fe(IV) reacts with another molecule of Fe(IV) and dimerizes which immediately self-decays to form two molecules of Fe(III) and H₂O₂. One molecule from the remaining Fe(IV) reacts with H₂O₂ to form Fe(II). This Fe(II) now reacts with Fe(VI) and Fe(IV) to generate Fe(V) and Fe(III),

respectively, via one-electron transfer pathways. The unused Fe(II) further reacts with H₂O₂ to form more Fe(IV). Fe(V) also undergoes self-decay to form Fe(III) and H₂O₂. Fe(V) further reacts with the H₂O₂ to form Fe(III) and one molecule of oxygen (Eq. 10).

Table 6 Proposed Reactions in the Fe(VI)-PAA-substrate system

Reactions	<i>k</i> at pH 9.0	Reference
[1] Fe ^{VI} O ₄ ²⁻ + H ₂ O → Fe ^{IV} O ₃ ²⁻ + H ₂ O ₂	2.0×10 ⁻⁵ s ⁻¹	Estimated in Fe(VI) decay system
[2] Fe ^{VI} O ₄ ²⁻ + H ₂ O ₂ → Fe ^{IV} O ₃ ²⁻ + O ₂ + H ₂ O	~ 0 M ⁻¹ s ⁻¹	38
[3] Fe ^{IV} O ₃ ²⁻ + Fe ^{IV} O ₃ ²⁻ → Fe ₂ ^{IV} O ₆ ⁴⁻	~ 10 ⁷ M ⁻¹ s ⁻¹	39
[4] Fe ₂ ^{IV} O ₆ ⁴⁻ + 4 H ₂ O + 4 H ⁺ → 2Fe ^{III} (OH) ₃ (H ₂ O) + H ₂ O ₂	10 ² s ⁻¹	39
[5] Fe ^{IV} O ₃ ²⁻ + H ₂ O ₂ + 2 H ⁺ → Fe ^{II} (OH) ₂ (aq) + O ₂ + 2 H ₂ O	3.0×10 ³ M ⁻¹ s ⁻¹	39, 40
[6] Fe ^{IV} O ₃ ²⁻ + Fe ^{II} (OH) ₂ (aq) + 3 H ₂ O → 2 Fe ^{III} (OH) ₃ (aq) + 2 OH ⁻	~ 10 ⁶ M ⁻¹ s ⁻¹	39
[7] Fe ^{VI} O ₄ ²⁻ + Fe ^{II} (OH) ₂ (aq) + H ₂ O → HFe ^V O ₄ ²⁻ + Fe ^{III} (OH) ₃ (aq)	~ 10 ⁵ M ⁻¹ s ⁻¹	22, 41
[8] Fe ^{II} (OH) ₂ (aq) + H ₂ O ₂ + 2 OH ⁻ → Fe ^{IV} O ₃ ²⁻ + 3 H ₂ O	~ 10 ³ M ⁻¹ s ⁻¹	42
[9a] HFe ^V O ₄ ²⁻ + 2 H ⁺ + 4 H ₂ O → Fe ^{III} (OH) ₃ (H ₂ O) ₃ + H ₂ O ₂	5.0 s ⁻¹	43
[9b] HFe ^V O ₄ ²⁻ + HFe ^V O ₄ ²⁻ + 4 H ₂ O + 4 H ⁺ → 2 Fe ^{III} (OH) ₃ (H ₂ O) + 2 H ₂ O ₂	1.5×10 ⁷ M ⁻¹ s ⁻¹	44

[10] $\text{HFe}^{\text{V}}\text{O}_4^{2-} + \text{H}_2\text{O}_2 + \text{H}_2\text{O} \rightarrow \text{Fe}^{\text{III}}(\text{OH})_3(\text{aq}) + \text{O}_2 + 2 \text{OH}^-$	$4.0 \times 10^5 \text{M}^{-1} \text{s}^{-1}$	38
[11] $\text{Fe}^{\text{VI}}\text{O}_4^{2-} + \text{CH}_3\text{CO}_3^- \rightarrow \text{Fe}^{\text{IV}}\text{O}_3^{2-} + \text{CH}_3\text{CO}_2^- + \text{O}_2$	$58 \pm 1.0^* \text{M}^{-1} \text{s}^{-1}$	Estimated in this study
[12] $\text{Fe}^{\text{IV}}\text{O}_3^{2-} + \text{ATL} \rightarrow \text{Fe}^{\text{III}}(\text{OH})_3(\text{aq}) + \text{P1}$	$(1.85 \pm 0.3) \times 10^5 \text{M}^{-1} \text{s}^{-1}$	Estimated in this study
[13] $\text{Fe}^{\text{IV}}\text{O}_3^{2-} + \text{CAF} \rightarrow \text{Fe}^{\text{III}}(\text{OH})_3(\text{aq}) + \text{P1}$	$(1.5 \pm 0.1) \times 10^5 \text{M}^{-1} \text{s}^{-1}$	Estimated in this study
[14] $\text{Fe}^{\text{IV}}\text{O}_3^{2-} + \text{PPN} \rightarrow \text{Fe}^{\text{III}}(\text{OH})_3(\text{aq}) + \text{P1}$	$(3.35 + 0.05) \times 10^5 \text{M}^{-1} \text{s}^{-1}$	Estimated in this study
[15] $\text{Fe}^{\text{IV}}\text{O}_3^{2-} + \text{SDM} \rightarrow \text{Fe}^{\text{III}}(\text{OH})_3(\text{aq}) + \text{P1}$	$(3.0 \pm 0.3) \times 10^5 \text{M}^{-1} \text{s}^{-1}$	Estimated in this study
[16] $\text{Fe}^{\text{IV}}\text{O}_3^{2-} + \text{SMX} \rightarrow \text{Fe}^{\text{III}}(\text{OH})_3(\text{aq}) + \text{P1}$	$(2.72 \pm 0.2) \times 10^5 \text{M}^{-1} \text{s}^{-1}$	Estimated in this study
[17] $\text{Fe}^{\text{IV}}\text{O}_3^{2-} + \text{TMP} \rightarrow \text{Fe}^{\text{III}}(\text{OH})_3(\text{aq}) + \text{P1}$	$(1.56 + 0.1) \times 10^5 \text{M}^{-1} \text{s}^{-1}$	Estimated in this study
[18] $\text{Fe}^{\text{VI}}\text{O}_4^{2-} + \text{ATL} \rightarrow \text{Fe}^{\text{III}}(\text{OH})_3(\text{aq}) + \text{P2}$	$12.0 \text{M}^{-1} \text{s}^{-1}$	Estimated in this study
[19] $\text{Fe}^{\text{VI}}\text{O}_4^{2-} + \text{CAF} \rightarrow \text{Fe}^{\text{III}}(\text{OH})_3(\text{aq}) + \text{P2}$	$6.7 \text{M}^{-1} \text{s}^{-1}$	Estimated in this study
[20] $\text{Fe}^{\text{VI}}\text{O}_4^{2-} + \text{PPN} \rightarrow \text{Fe}^{\text{III}}(\text{OH})_3(\text{aq}) + \text{P2}$	$2.0 \text{M}^{-1} \text{s}^{-1}$	Estimated in this study
[21] $\text{Fe}^{\text{VI}}\text{O}_4^{2-} + \text{SDM} \rightarrow \text{Fe}^{\text{III}}(\text{OH})_3(\text{aq}) + \text{P2}$	$5.7 \text{M}^{-1} \text{s}^{-1}$	Estimated in this study
[22] $\text{Fe}^{\text{VI}}\text{O}_4^{2-} + \text{SMX} \rightarrow \text{Fe}^{\text{III}}(\text{OH})_3(\text{aq}) + \text{P2}$	$12.3 \text{M}^{-1} \text{s}^{-1}$	Estimated in this study
[23] $\text{Fe}^{\text{VI}}\text{O}_4^{2-} + \text{TMP} \rightarrow \text{Fe}^{\text{III}}(\text{OH})_3(\text{aq}) + \text{P2}$	$5.2 \text{M}^{-1} \text{s}^{-1}$	Estimated in this study

**Standard deviation estimated by using the standard deviation generated by the fit data function on matlab*

3.2.2 Kinetic Simulation of Fe(VI) decay by PAA – Eq. 11

Experimental data were obtained by Dr. Sharma's group which include (i) Fe(VI) decay in the presence of PAA, (ii) substrate degradation by PAA alone, (iii) substrate degradation by Fe(VI) alone, and (iv) substrate degradation by Fe(VI)/PAA. The kinetic model for this system at pH 9.0 includes the reactions listed in Table 4.

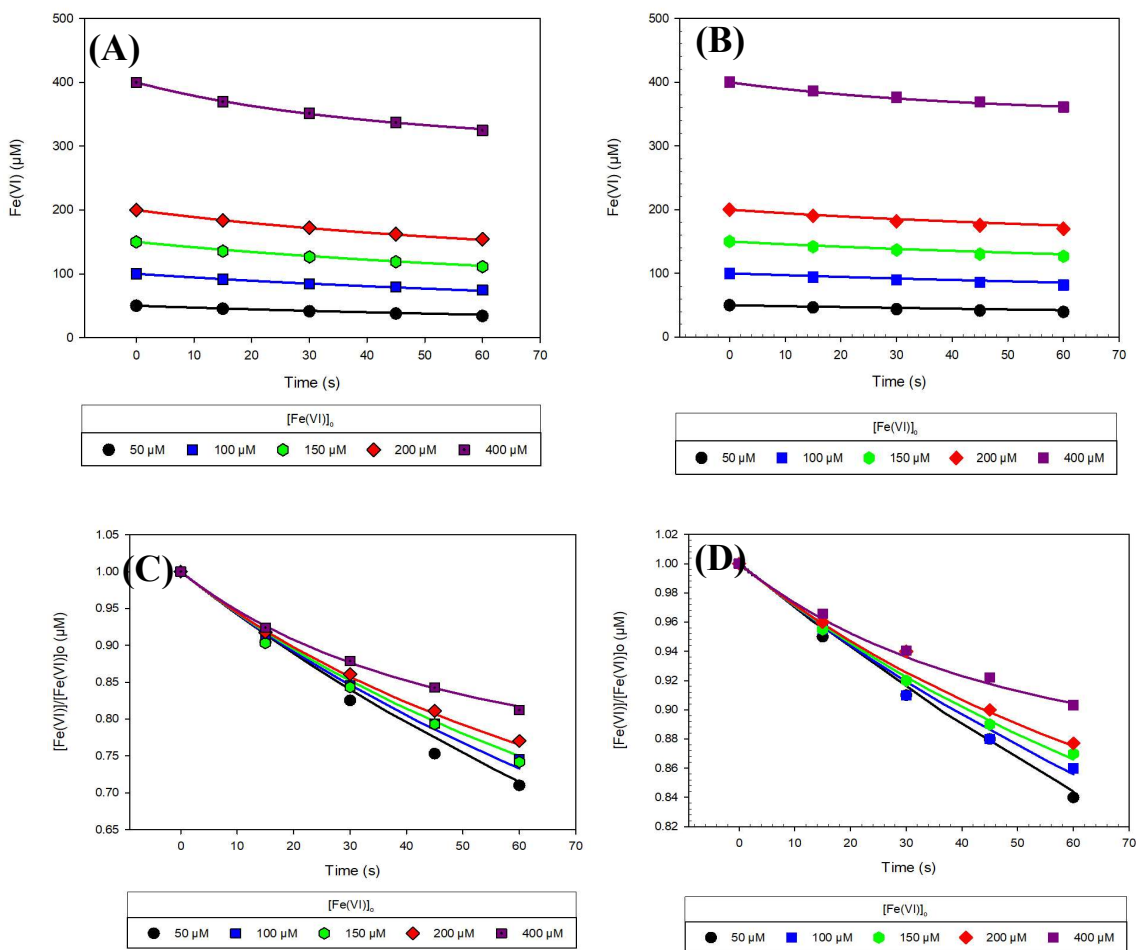


Figure 7. Experimental data and kinetic simulation of Fe(VI) decay in the Fe(VI)-PAA system. Solid symbols: experimental data for Fe(VI) decay. (Experimental conditions: $[Fe(VI)]_0 = 50.0-400.0 \mu$ M, $[PAA]_0 = 100.0 \mu$ M (A)(C) and 50.0μ M (B)(D), 10.0 mM borate buffer, and pH = 9.0). Line: model simulation.

Eq. 11 was added to investigate the reaction of Fe(VI) with PAA. We proposed Fe(IV) to be the major reactive species and hence explored to model the Fe(VI) decay and substrate decay using Eq. 11, that is Fe(VI) reacting with PAA to form Fe(IV), acetic acid and one molecule of oxygen. As shown in Figure 7, by fitting to the experimental data for Fe(VI)

decay by two different concentrations of PAA (50 μM and 100 μM), k_{11} was estimated to be $58 \pm 1.0 \text{ M}^{-1}\cdot\text{s}^{-1}$.

3.2.3 Kinetic Simulation of Substrate Degradation (Eq. 12-23)

For each substrate, Fe(IV) and Fe(VI) in the system were proposed to react with the compound (Eqs. 12-23). From the experiments conducted, we got the data for the degradation of the substrates by only PAA and only Fe(VI). To have a good estimate/range of the rate constants of Fe(VI) with substrates, the data of substrate degradation with only Fe(VI) were considered to derive the second-order rate constant from the psuedo-first order rate constant. This gives good estimates of the rate constants of Fe(VI) with the pharmaceutical micropollutant ($k_{18-23} = 2.0\text{-}12.3 \text{ M}^{-1}\cdot\text{s}^{-1}$) which agree with the range of reported values from previous literature.²³

Obtaining/fixing the rate constant of substrates with Fe(VI) and then modeling for the experimental data helps us estimate the rate constant for Fe(IV) with substrates in the Fe(VI)-PAA-substrate system. Eqs. 12-17 are the reaction of Fe(IV) for each of the substrate considered. The estimated rate constants for Fe(IV) with micropollutants from the kinetic modeling are in the range of $(1.56\text{-}3.35) \times 10^5 \text{ M}^{-1}\cdot\text{s}^{-1}$ (Table 4).

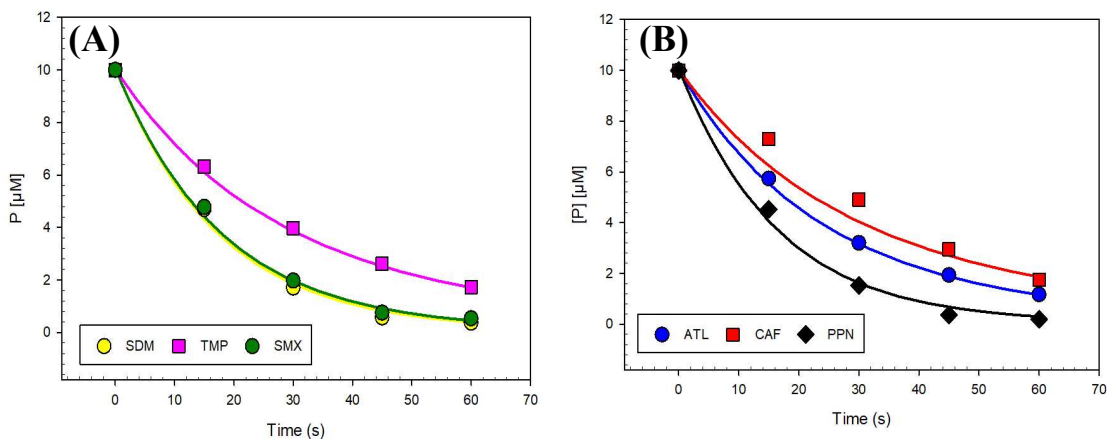


Figure 8. Experimental data and kinetic simulation of degradation of substrates in the Fe(VI)-PAA-substrate system. Experimental conditions: $[\text{Fe(VI)}]_0 = 200.0 \mu\text{M}$, $[\text{PAA}]_0 = 100.0 \mu\text{M}$, $[\text{pharmaceutical}]_0 = 10.0 \mu\text{M}$, $\text{pH} = 9.0 \pm 0.1$, 10.0 mM borate buffer, $T = 25 \pm 1 \text{ }^\circ\text{C}$. (A) Antibiotics: SMX-sulfamethoxazole, SDM-sulfadimethoxine, and TMP-trimethoprim. (B) Beta blockers: ATL-atenolol, and PPN-propranolol. Stimulant: CAF-caffeine.

The estimated rate constants for the Fe(IV)-micropollutant study correlates well with the prediction in previous studies. Although reported rate constants with Fe(IV) were not available for all the micropollutants considered in this study, the order of magnitude of the reaction rate constants of Fe(IV) with similar organic compounds were in the higher range of $10^4 \text{ M}^{-1}\text{s}^{-1}$,^{12,23} which compare well with the lower $10^5 \text{ M}^{-1}\text{s}^{-1}$ values obtained in this study.

3.2.4 Goodness-of-fit

The goodness of fit to see how well the model was able to predict the trends in comparison to experimental data was computed using the Thiel's inequality coefficient, NRMSE and ME. The results are tabulated in Table 5. All three methods were well within the limits, thus validating the model's ability to predict the reaction kinetics well. According to previous studies a value of TIC lower than 0.3^{28,29,35} and a ME^{29,36} around 1.0 indicated a good fit of the two sets of data under consideration.

Table 7. Goodness-of-fit test for the Fe(VI)-PAA system for Fe(VI) decay prediction

[PAA] ₀	[Fe(VI)] ₀	TIC	NRSME	ME
50	50	2.0×10^{-4}	0.20	0.44
	100	4.1×10^{-4}	0.13	0.78
	150	6.2×10^{-4}	0.11	0.87
	200	8.3×10^{-4}	0.11	0.85
	400	1.7×10^{-3}	0.03	0.99
100	50	2.0×10^{-4}	0.06	0.95

100	3.8×10^{-4}	0.03	0.99
150	5.8×10^{-4}	0.03	0.99
200	7.8×10^{-4}	0.02	0.98
400	1.6×10^{-3}	0.01	1.00

Table 8. Goodness-of-fit test for the Fe(VI)-PAA system for substrate decay prediction

Condition	[Fe(VI)] _o	TIC	NRSME	ME
[PAA] _o = 200μM	ATL	2.4×10^{-5}	6×10^{-3}	1.0
[Fe(VI)] _o = 100μM	CAF	2.8×10^{-5}	2×10^{-3}	1.0
Substrate = 10μM	PPN	2.2×10^{-5}	7×10^{-3}	1.0
	SDM	2.3×10^{-5}	5×10^{-3}	1.0
	SMX	2.3×10^{-5}	2×10^{-3}	1.0
	TMP	2.6×10^{-5}	6×10^{-3}	1.0

3.3 Conclusion

This study was a modeling effort toward investigating the Fe(VI)-PAA system with and without micropollutant substrates. The focus was on the reaction of Fe(VI) with PAA to generate Fe(IV) and the degradation reactions of substrates by Fe(VI) and Fe(IV). Goodness-of-fit tests validate the kinetic model in consideration. Although the formation of Fe(V) was much lower than Fe(IV) in this system, future work can study the Fe(V) generation and the impact it has on substrate degradation. In addition, quantum chemical

computation such as density functional theory calculations (DFT) should be conducted in the future to provide confirmation for the dominant role of Fe(IV) proposed by this study for the Fe(VI)-PAA system.

CHAPTER 4. FE(VI)–DMA SYSTEM

4.1 Methodology

4.1.1 Chemicals

Amines (i.e., MMA, DMA, and TMA), hydroxylamine, methyl phenyl sulfoxide (PMSO), methyl phenyl sulfone (PMSO₂), and Na₂B₄O₇·10H₂O as well as methanol and phosphoric acid (85%) (high-performance liquid chromatography (HPLC) grades) were acquired from Fisher Scientific (Austin, Texas, USA) and were used without further purification. A wet chemical synthesis method was applied to synthesize potassium ferrate at a purity > 95%.³⁷ The stock solutions of Fe^{VI}, amines, PMSO, and hydroxylamine were prepared in 10.0 mM Na₂B₄O₇ at pH 9.0.

All chemicals were of 97% or greater purity and utilized without additional purification. Reagent – grade deionized water (DI) with a resistivity lesser than 18 mΩ-cm was used from a Nanopure Millipore (Billerica, MA) water purification system.

All experimental data were obtained from Dr. Virender Sharma's Laboratory at the Texas A&M University.

4.1.2 Kinetic Modeling

A modeling was attempted for the Fe(VI)–DMA system using the equations listed in Table 7. The modeling was carried out to study the mechanism involved in the Fe(VI)–DMA–substrate oxidation system. The Fe(VI) decay without the substrate was also monitored and modeled.

4.2 Results and Discussion

Experimental data for Fe(VI) decay in the presence of dimethylamine (DMA) were obtained at pH 9 from Dr. Sharma's group. Fe(VI) decay by DMA was simulated for the

first 5 seconds of the reaction. Eqs. 1-12 in Table 9 were proposed to simulate the Fe(VI) decay. In this model, the self-decay reactions of Fe(VI) was described in Eqs. 1-10, as mentioned in the Fe(VI)-PAA section. Eqs 11 and 12 represent the two major reaction pathways from the impact of DMA, i.e., the reaction of Fe(VI) with DMA and the reaction of Fe(IV) with DMA, respectively.

Table 9. Proposed reactions for the Fe(VI)-DMA system at pH 9.

Reactions	<i>k</i> at pH 9.0	Reference
[1] $\text{Fe}^{\text{VI}}\text{O}_4^{2-} + \text{H}_2\text{O} \rightarrow \text{Fe}^{\text{IV}}\text{O}_3^{2-} + \text{H}_2\text{O}_2$	$4.8 \times 10^{-5} \text{ s}^{-1}$	45
[2] $\text{Fe}^{\text{VI}}\text{O}_4^{2-} + \text{H}_2\text{O}_2 \rightarrow \text{Fe}^{\text{IV}}\text{O}_3^{2-} + \text{O}_2 + \text{H}_2\text{O}$	$\sim 0 \text{ M}^{-1}\text{s}^{-1}$	38
[3] $\text{Fe}^{\text{IV}}\text{O}_3^{2-} + \text{Fe}^{\text{IV}}\text{O}_3^{2-} \rightarrow \text{Fe}_2^{\text{IV}}\text{O}_6^{4-}$	$\sim 10^7 \text{ M}^{-1}\text{s}^{-1}$	39
[4] $\text{Fe}_2^{\text{IV}}\text{O}_6^{4-} + 4 \text{ H}_2\text{O} + 4 \text{ H}^+ \rightarrow 2 \text{ Fe}^{\text{III}}(\text{OH})_3(\text{H}_2\text{O}) + \text{H}_2\text{O}_2$	10^2 s^{-1}	39
[5] $\text{Fe}^{\text{IV}}\text{O}_3^{2-} + \text{H}_2\text{O}_2 + 2 \text{ H}^+ \rightarrow \text{Fe}^{\text{II}}(\text{OH})_2(\text{aq}) + \text{O}_2 + 2 \text{ H}_2\text{O}$	$3.0 \times 10^3 \text{ M}^{-1}\text{s}^{-1}$	39,40
[6] $\text{Fe}^{\text{IV}}\text{O}_3^{2-} + \text{Fe}^{\text{II}}(\text{OH})_2(\text{aq}) + 3 \text{ H}_2\text{O} \rightarrow 2 \text{ Fe}^{\text{III}}(\text{OH})_3(\text{aq}) + 2 \text{ OH}^-$	$\sim 10^6 \text{ M}^{-1}\text{s}^{-1}$	39
[7] $\text{Fe}^{\text{VI}}\text{O}_4^{2-} + \text{Fe}^{\text{II}}(\text{OH})_2(\text{aq}) + \text{H}_2\text{O} \rightarrow \text{HFe}^{\text{V}}\text{O}_4^{2-} + \text{Fe}^{\text{III}}(\text{OH})_3(\text{aq})$	$\sim 10^5 \text{ M}^{-1}\text{s}^{-1}$	22,41
[8] $\text{Fe}^{\text{II}}(\text{OH})_2(\text{aq}) + \text{H}_2\text{O}_2 + 2 \text{ OH}^- \rightarrow \text{Fe}^{\text{IV}}\text{O}_3^{2-} + 3 \text{ H}_2\text{O}$	$\sim 10^3 \text{ M}^{-1}\text{s}^{-1}$	42
[9a] $\text{HFe}^{\text{V}}\text{O}_4^{2-} + 2 \text{ H}^+ + 4 \text{ H}_2\text{O} \rightarrow \text{Fe}^{\text{III}}(\text{OH})_3(\text{H}_2\text{O})_3 + \text{H}_2\text{O}_2$	5.0 s^{-1}	43
[9b] $\text{HFe}^{\text{V}}\text{O}_4^{2-} + \text{HFe}^{\text{V}}\text{O}_4^{2-} + 4 \text{ H}_2\text{O} + 4 \text{ H}^+ \rightarrow 2 \text{ Fe}^{\text{III}}(\text{OH})_3(\text{H}_2\text{O}) + 2 \text{ H}_2\text{O}_2$	$1.5 \times 10^7 \text{ M}^{-1}\text{s}^{-1}$	44

[10]	$\text{HFe}^{\text{V}}\text{O}_4^{2-} + \text{H}_2\text{O}_2 + \text{H}_2\text{O} \rightarrow \text{Fe}^{\text{III}}(\text{OH})_3(\text{aq}) + \text{O}_2 + 2 \text{OH}^-$	$4.0 \times 10^5 \text{ M}^{-1}\text{s}^{-1}$	38
[11]	$\text{Fe}^{\text{VI}}\text{O}_4^{2-} + \text{DMA} \rightarrow \text{Fe}^{\text{IV}}\text{O}_3^{2-} + \text{P}_1$	$13 \text{ M}^{-1}\text{s}^{-1}$	Derived in the Fe(VI)-DMA system
[12]	$\text{Fe}^{\text{IV}}\text{O}_4^{2-} + \text{DMA} \rightarrow \text{Fe}^{\text{II}}\text{O}_3^{2-} + \text{P}_2$	$50 \text{ M}^{-1}\text{s}^{-1}$	Derived in the Fe(VI)-DMA system

Figure 9 shows the kinetic simulation of the experimental data of Fe(VI) decay during the first 0-5 s of the reaction using the kinetic model, which estimated k_{11} and k_{12} values of $13 \text{ M}^{-1}\text{s}^{-1}$ and $50 \text{ M}^{-1}\text{s}^{-1}$, respectively.

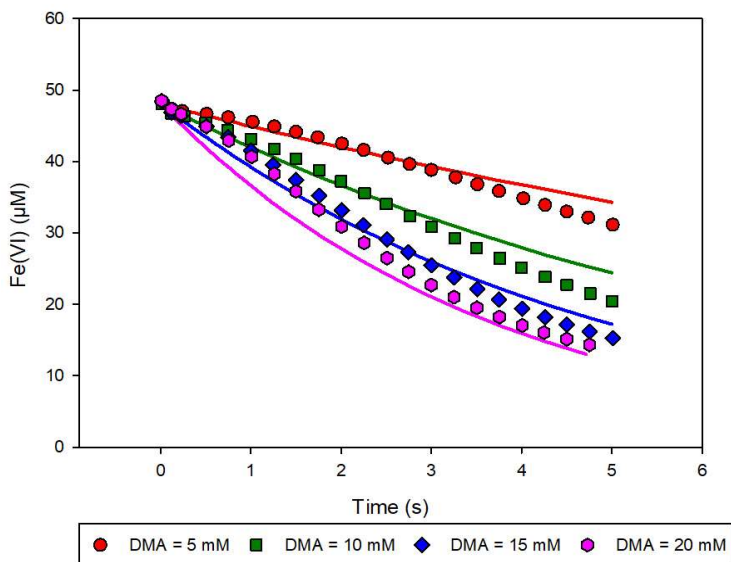


Figure 9. Experimental data and kinetic simulation of Fe(VI) decay in the Fe(VI)-DMA system for 5 seconds. Solid symbol: experimental data for Fe(VI) decay by DMA. Experimental conditions: $[\text{DMA}]_0 = 5.0 - 20.0 \text{ mM}$, $[\text{Fe(VI)}]_0 = 50.0 \text{ }\mu\text{M}$, $\text{pH} = 9.0$, 10.0 mM borate buffer. Line: model simulation.

As seen in Figure 10, the experimental data show that Fe(VI) did not completely decay in 12-30 seconds even in the presence of excess DMA (i.e., $[\text{DMA}]_0/[\text{Fe(VI)}]_0 = 100-400$),. The current model overestimates the Fe(VI) decay in the longer time range as shown in

Figure 11, since the proposed model does not contain any competitive reactions for DMA to be consumed before reacting with Fe(VI) completely.

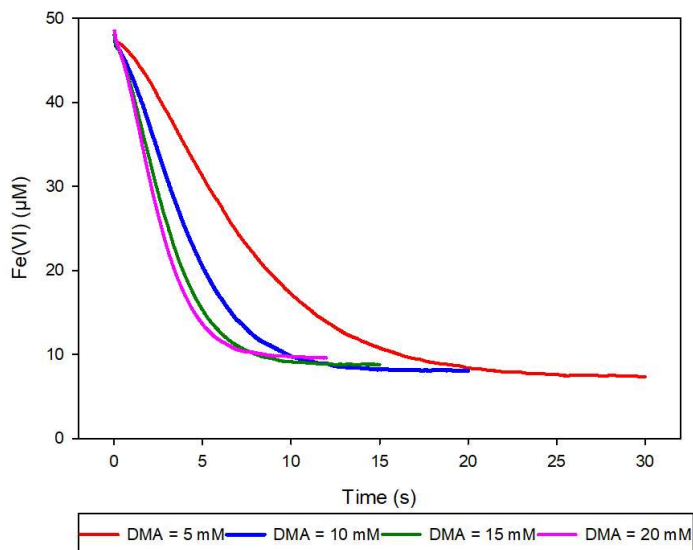
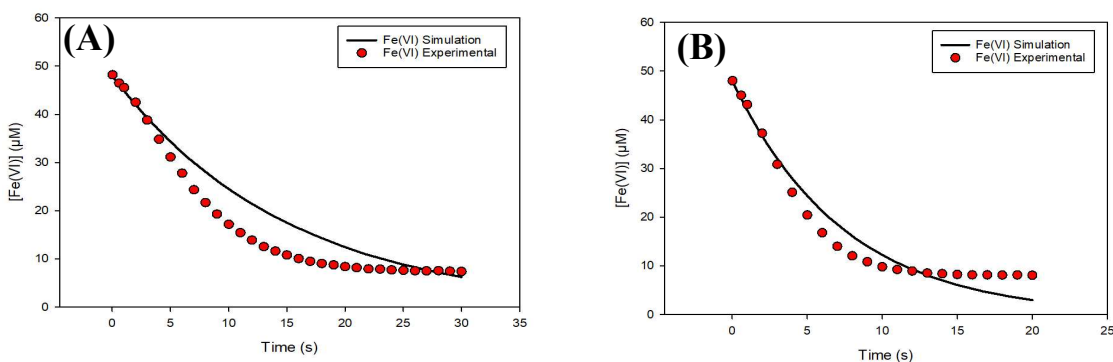


Figure 10. Experimental data of Fe(VI) decay in the Fe(VI)/DMA system for 30 seconds. (Experimental condition: $[DMA]_0 = 5.0 - 20.0$ mM, $[Fe(VI)] = 50.0$ μ M, pH = 9.0, 10.0 mM borate buffer). Note: The data appear as lines due to numerous data points collected frequently by the stopped-flow spectrometer.



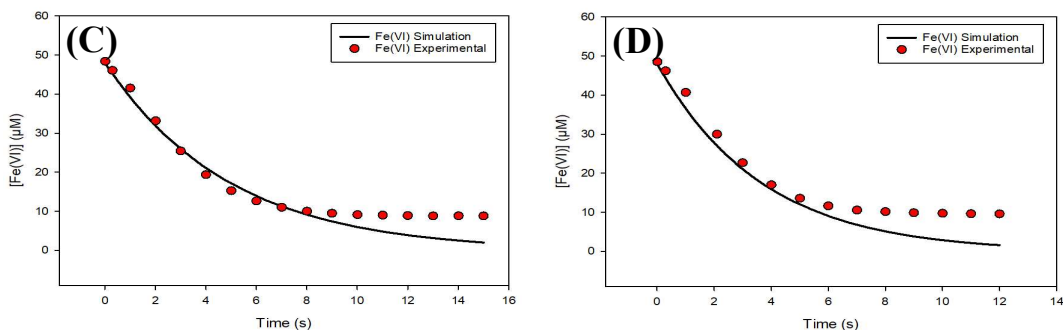


Figure 11. Kinetic Simulation of Fe(VI) decay at different DMA concentrations: A) 5mM B) 10mM C) 15mM D) 20mM. Solid symbol: experimental data for Fe(VI) decay by DMA. Line: model simulation. (Experimental condition: $[DMA]_0 = 5.0 - 20.0 \text{ mM}$, $[Fe(VI)] = 50.0 \text{ }\mu\text{M}$, $\text{pH} = 9.0$, 10.0 mM borate buffer).

The above results show that the Fe(VI) decay by DMA can be reasonably well predicted by the proposed kinetic model for the first 5 seconds. However, the simulated data over a longer time period show a large deviation from the measured data. We hypothesize the following two potential causes for the discrepancy between the theoretical kinetic model calculation and the experimental data:

1. *Analytical interference*: The Fe(VI) decay was measured using a stopped-flow spectrophotometer at 510 nm. Fe(III) formed from the decay of Fe(VI) has a weak absorbance at this wavelength. Furthermore, oxidation products of DMA and iron complexes of DMA and/or DMA products may contribute to absorbance in the same region of 510 nm. This analytical interference, if occurs, will lead to the appearance of incomplete decay of Fe(VI).
2. *Amine intermediate interference*: The oxidative intermediate of DMA may form complexes with Fe(VI) or Fe(IV) which may stabilize these species in the solution and result in the plateauing trend of Fe(VI) decay. A “stabilizing” effect of amine oxidation products for reactive iron species could be a possible explanation for the incomplete decay of Fe(VI).

Figure 12 shows the enhanced degradation of TMP in the Fe(VI)-DMA system, compared to the degradation of TMP by Fe(VI) without the DMA activator. To model the enhanced

TMP decay in the Fe(VI)-DMA-TMP system, the rate constant values of k_{11} and k_{12} estimated for the 0-5 s were used. As Figure 12 shows, the model was not successful to capture the TMP's decay trends. This was likely due to the inability of the model to fully account for the possibly complicated effects of DMA.

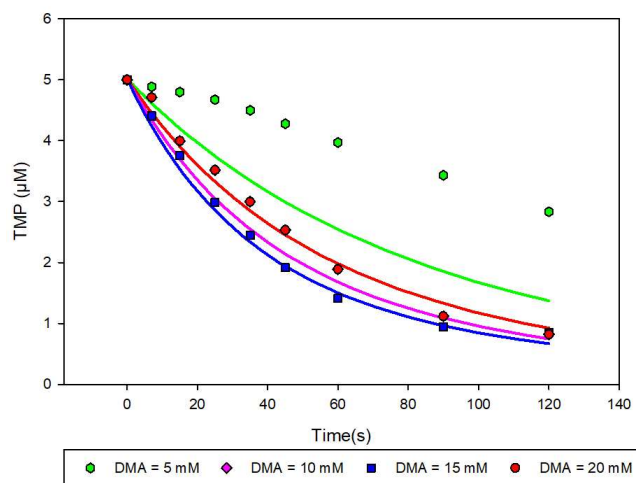


Figure 12. Experimental data and kinetic simulation of TMP decay in the Fe(VI)-DMA system at different DMA concentrations: A) 5 mM B) 10 mM C) 15 mM D) 20 mM. Solid symbol: experimental data for TMP decay by DMA. Line: model simulation. (Experimental condition: $[DMA]_0 = 5.0 - 20.0$ mM, $[Fe(VI)]_0 = 50.0$ μ M, pH = 9.0, 10.0 mM borate buffer).

4.3 Conclusion

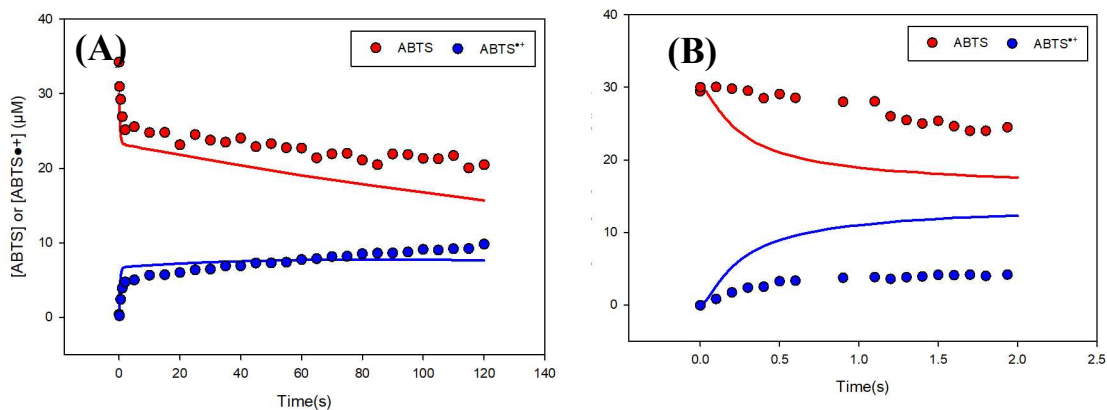
This study was an effort to model the kinetics of the Fe(VI)-DMA-micropollutant system. The current model requires many improvements in order to address the limitations faced. Future research should be explored to resolve the possible causes for the changing kinetic behaviors of Fe(VI) decay in the presence of DMA over time, and to build a more comprehensive and robust model to predict the decay of Fe(VI) and contaminant in the presence of amine activators. In addition, quantum chemical computation such as density functional theory calculations (DFT) could be used simultaneously to provide better clarity in the involvement of species in this complicated system.

APPENDIX A.

Additional Experiments and Kinetic Modeling for the Fe(II)-PAA-ABTS system:

The conditions where $[PAA]_0$ is equal to $[Fe(II)]_0$ and $[PAA]_0$ is lower than $[Fe(II)]_0$, i.e., $[PAA]_0 = 50 \mu\text{M}$, $[Fe(II)]_0 = 50 \mu\text{M}$, $[ABTS]_0 = 25 \mu\text{M}$ and $[PAA]_0 = 25 \mu\text{M}$, $[Fe(II)]_0 = 50 \mu\text{M}$, $[ABTS]_0 = 25 \mu\text{M}$ were also considered for this system. Experimental data were obtained using similar methods for the previous conditions and simulations were carried out using the same model with equations as listed in Chapter 2.

The results of these systems were as shown in Figure below.



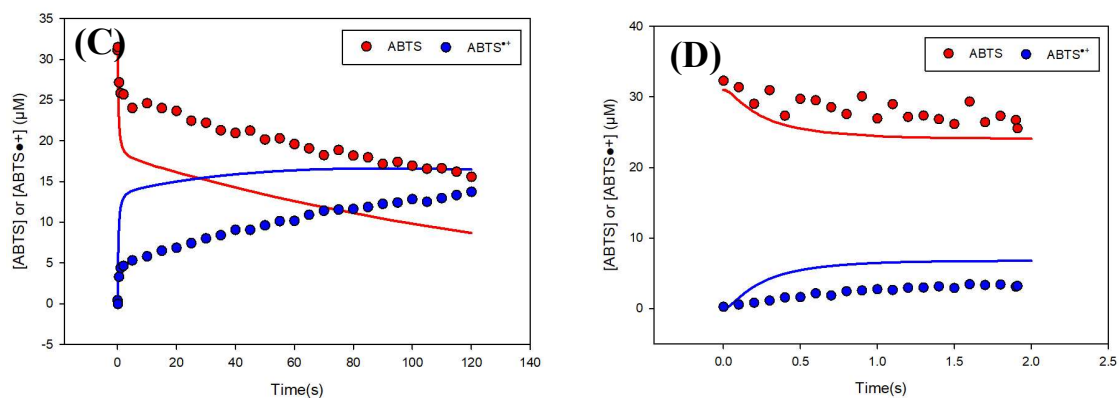


Figure A.1. Experimental data and kinetic simulation of ABTS and ABTS^{•+} at A), C) 120 s B), D) 2s. Solid Symbol: ABTS and ABTS^{•+} experimental data points. Line: Model Simulation (Experimental Conditions: A) B) [PAA]_o = 50 μM, [Fe(II)]_o = 50 μM, [ABTS]_o = 25 μM, [H₂O₂]_o = 31 μM, C) D) [PAA]_o = 25 μM, [Fe(II)]_o = 50 μM, [ABTS]_o = 25 μM, [H₂O₂]_o = 31 μM

As seen from the results, the current model overestimates both the consumption of ABTS and the generation of ABTS^{•+}. Changing the ratio of the rate constants (k_{1a}/k_{1b}) results in a better fitting of the data but the reason to change the ratio is still not clear. More experiments are required to investigate the mechanisms involved in this system.

In addition to the above trends, the PAA decay for different conditions were modeled to see if any other PAA sink was involved in the system. But results suggest that no other reaction was involved in PAA decay.

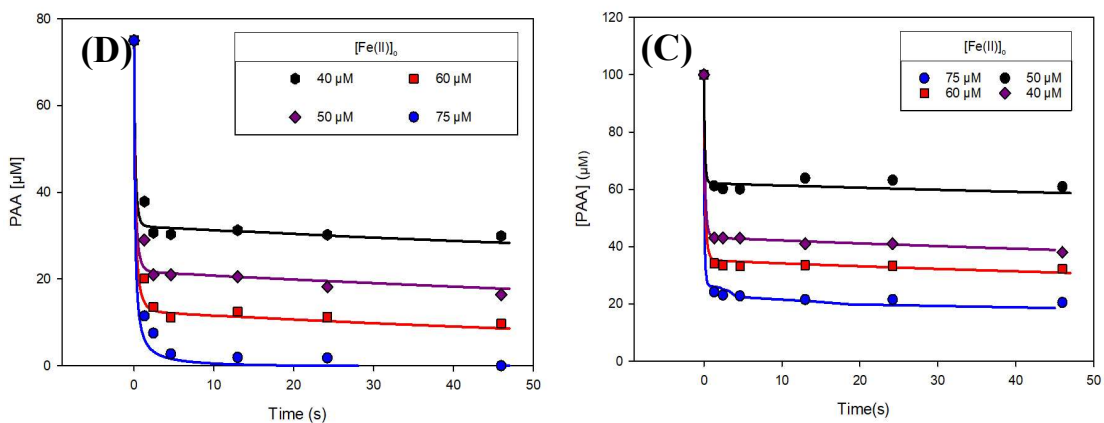


Figure A. 2 Experimental data and kinetic simulation of PAA in reaction conditions, A: $[\text{PAA}]_0 = 100 \mu\text{M}$, $[\text{Fe(II)}]_0 = 75, 60, 50, 40 \mu\text{M}$, $[\text{ABTS}]_0 = 25 \mu\text{M}$, B: $[\text{PAA}]_0 = 75 \mu\text{M}$, $[\text{Fe(II)}]_0 = 75, 60, 50, 40 \mu\text{M}$, $[\text{ABTS}]_0 = 25 \mu\text{M}$. $[\text{H}_2\text{O}_2]_0 = 31 \mu\text{M}$ for all. Solid Symbol: Experimental data. Line: Model Simulation

Sensitivity Analysis Coefficients: The sensitivity coefficients of all conditions are tabulated here.

Table A.1. Sensitivity Coefficients at [PAA]_o = 100 μM, [Fe(II)]_o = 50 μM, [ABTS]_o = 25 μM, t = 2 s

Rate Constant	Sensitivity Coefficient								Overall
	PAA	Fe(II)	Fe(IV)	ABTS ^{•+}	ABTS	CH ₃ CO ₂ [•]	CH ₃ COOO [•]	Fe(OH) ₃	
k_{1a}	0.18	4.7	5.0	0.93	0.9	2.8	4.8	0.2	19.5
k_{1b}	0.26	0.82	2.2	1.3	1.1	1.1	2.7	3.8×10 ⁻²	9.48
k₂	4.5×10 ⁻⁴	1.3×10 ⁻³	2.3×10 ⁻³	2.3×10 ⁻³	1.2×10 ⁻³	7.2×10 ⁻⁴	7.6	5.9×10 ⁻⁵	7.6
k₃	0.15	1.1	2.5	0.63	0.47	1.0	0.87	6.1×10 ⁻²	6.72
k₄	3.4×10 ⁻³	0.33	0.23	1.4×10 ⁻²	1.4×10 ⁻²	0.32	0.78	3.0×10 ⁻²	1.66
k₅	3.5×10 ⁻⁹	9.9×10 ⁻⁹	2.5×10 ⁻⁸	4.0×10 ⁻⁵	2.0×10 ⁻⁸	6.4×10 ⁻⁹	2.2	1.5×10 ⁻⁶	2.2
k₆	3.3×10 ⁻⁴	1.0×10 ⁻³	2.3×10 ⁻³	2.8×10 ⁻³	1.6×10 ⁻³	2.0	3.5	4.0×10 ⁻⁴	5.5
k₇	9.4×10 ⁻²	9.2×10 ⁻²	5.0×10 ⁻²	2.9×10 ⁻²	2.6×10 ⁻²	8.2×10 ⁻¹	1.1	1.8×10 ⁻³	1.1
k₈	1.4×10 ⁻⁴	7.1×10 ⁻⁴	1.7×10 ⁻³	7.6×10 ⁻⁴	6.7×10 ⁻⁴	5.7×10 ⁻⁴	0.43	4.7×10 ⁻⁵	0.43
k₉	1.9×10 ⁻⁵	1.3×10 ⁻⁴	5.0×10 ⁻⁴	6.6×10 ⁻²	3.7×10 ⁻⁴	9.8×10 ⁻⁵	0.92	1.7×10 ⁻⁵	0.92
k₁₀	0.11	0.5	0.72	0.25	0.22	0.4	1.6	2.5×10 ⁻²	3.8
k₁₁	1.4×10 ⁻⁴	5.1×10 ⁻⁴	4.8×10 ⁻⁴	1.0×10 ⁻⁴	9.3×10 ⁻⁵	4.0×10 ⁻⁴	1.1	6.1×10 ⁻⁵	1.1
k₁₂	6.4×10 ⁻⁴	7.5×10 ⁻³	6.5×10 ⁻³	2.9×10 ⁻³	4.5×10 ⁻⁴	6.9×10 ⁻³	1.2	2.1×10 ⁻⁴	1.2
k₁₃	0.25	1.0	0.32	0.28	0.24	0.82	1.5	2.5×10 ⁻²	4.41

Table A.2. Sensitivity Coefficients at [PAA]_o = 100 μM, [Fe(II)]_o = 50 μM, [ABTS]_o = 25 μM, t = 2 s

Rate Constant	Sensitivity Coefficient								Overall
	PAA	Fe(II)	Fe(IV)	ABTS ^{•+}	ABTS	PAAr	CH ₃ COO [•] r	Fe(OH) ₃	
k _{1a}	11.3	35.4	74.9	36.7	75.6	103.0	390.3	2.0×10 ⁻¹	727.2
k _{1b}	12.6	94.0	69.0	40.8	82.8	107.4	427.6	3.8×10 ⁻²	834.2
k ₂	2.0×10 ⁻²	6.2×10 ⁻²	7.1×10 ⁻²	4.8×10 ⁻²	9.5×10 ⁻²	1.1×10 ⁻¹	70.1	5.9×10 ⁻⁵	70.1
k ₃	18.4	56.8	101.0	15.1	30.5	38.2	758.0	6.1×10 ⁻²	1018
k ₄	11.0	75.8	103.0	22.2	58.5	64.9	7599.0	3.0×10 ⁻²	7934.4
k ₅	5.4×10 ⁻⁵	2.0×10 ⁻³	4.7×10 ⁻³	6.2×10 ⁻⁴	1.6×10 ⁻³	1.8×10 ⁻²	4134.0	1.5×10 ⁻⁶	4134
k ₆	7.5×10 ⁻²	0.4	1.5×10 ⁻¹	2.8×10 ⁻¹	5.5×10 ⁻¹	119.5	91.9	4.0×10 ⁻⁴	211.8
k ₇	1.2	4.8	3.9	1.1	2.3	5.9	3.6×10 ⁵	1.9×10 ⁻³	19.2
k ₈	7.0×10 ⁻³	3.8×10 ⁻²	1.9×10 ⁻²	2.4×10 ⁻²	4.8×10 ⁻¹	6.8×10 ⁻¹	13.8	4.7×10 ⁻⁵	13.8
k ₉	1.5×10 ⁻³	3.0×10 ⁻²	1.0×10 ⁻²	1.7×10 ⁻²	3.4×10 ⁻²	1.9×10 ⁻¹	198.7	1.7×10 ⁻⁵	198.7
k ₁₀	7.9	7.9	9.1×10 ⁻³	8.1	16.3	15.7	111.0	2.5×10 ⁻²	166.9
k ₁₁	1.7×10 ⁻²	7.2×10 ⁻³	4.9	5.3×10 ⁻³	1.0×10 ⁻²	7.1×10 ⁻²	47.2	6.0×10 ⁻⁵	52.1
k ₁₂	8.4×10 ⁻²	3.0×10 ⁻¹	4.0×10 ⁻²	2.0×10 ⁻¹	6.7×10 ⁻²	2.2×10 ⁻¹	73.0	2.1×10 ⁻⁴	73
k ₁₃	24.0	50.0	18.9	9.2	18.8	25.5	174.6	2.5×10 ⁻²	321

Table A. 3 Sensitivity Coefficients at [PAA]_o = 100 μM, [Fe(II)]_o = 25 μM, [ABTS]_o = 10 μM, t = 2

Rate Constant	Sensitivity Coefficient								Overall
	PAA	Fe(II)	Fe(IV)	ABTS ^{•+}	ABTS	CH ₃ CO ₂ [•]	CH ₃ COOO [•]	Fe(OH) ₃	
k_{1a}	1.5×10 ⁻¹	5.6	5.2	1.0	6.9×10 ⁻¹	12.0	4.9	2.2×10 ⁻¹	29.8
k_{1b}	1.9×10 ⁻¹	9.4×10 ⁻¹	3.1	1.4	8.4×10 ⁻¹	3.3	1.7	2.1×10 ⁻²	11.7
k₂	2.2×10 ⁻⁴	1.6×10 ⁻³	2.5×10 ⁻³	3.9×10 ⁻³	1.4×10 ⁻³	3.6×10 ⁻³	4.1	3.4×10 ⁻⁵	4.1
k₃	9.3×10 ⁻²	1.8	2.7	8.8×10 ⁻¹	5.0×10 ⁻¹	1.7	1.2	4.7×10 ⁻²	8.9
k₄	7.5×10 ⁻⁴	2.4×10 ⁻¹	1.3×10 ⁻¹	9.2×10 ⁻³	6.5×10 ⁻³	2.4×10 ⁻¹	6.2×10 ⁻¹	1.6×10 ⁻²	1.3
k₅	5.8×10 ⁻⁹	3.8×10 ⁻⁸	5.1×10 ⁻⁸	9.3×10 ⁻⁵	4.7×10 ⁻⁸	3.6×10 ⁻⁸	2.3	3.2×10 ⁻⁹	2.3
k₆	2.0×10 ⁻⁴	1.6×10 ⁻⁴	2.5×10 ⁻³	4.3×10 ⁻³	1.6×10 ⁻³	2.0	5.2	3.3×10 ⁻⁵	7.2
k₇	2.2×10 ⁻³	2.6×10 ⁻²	1.5×10 ⁻¹	4.2×10 ⁻²	2.8×10 ⁻²	2.6×10 ⁻²	4.8×10 ⁻¹	5.2×10 ⁻⁴	0.75
k₈	1.1×10 ⁻⁴	1.6×10 ⁻⁴	2.4×10 ⁻³	8.5×10 ⁻⁴	5.7×10 ⁻⁴	1.5×10 ⁻³	5.5×10 ⁻¹	5.8×10 ⁻⁵	0.55
k₉	6.7×10 ⁻⁶	1.6×10 ⁻⁴	1.8×10 ⁻⁴	5.0×10 ⁻⁴	1.8×10 ⁻⁴	1.4×10 ⁻⁴	2.4×10 ⁻¹	3.4×10 ⁻⁶	0.24
k₁₀	3.8×10 ⁻²	3.6×10 ⁻¹	4.5×10 ⁻¹	1.6×10 ⁻¹	1.0×10 ⁻¹	3.2×10 ⁻¹	4.0×10 ⁻¹	1.7×10 ⁻²	1.8
k₁₁	3.0×10 ⁻⁵	1.8×10 ⁻⁴	2.7×10 ⁻⁴	5.7×10 ⁻⁵	3.8×10 ⁻⁵	1.7×10 ⁻⁴	2.7×10 ⁻¹	1.4×10 ⁻⁵	0.27
k₁₂	7.9×10 ⁻⁵	2.0×10 ⁻³	1.6×10 ⁻³	1.0×10 ⁻³	1.0×10 ⁻⁴	1.9×10 ⁻³	3.4×10 ⁻¹	2.8 ×10 ⁻⁵	0.34
k₁₃	1.3×10 ⁻¹	3.9×10 ⁻¹	1.6	5.0×10 ⁻¹	3.3×10 ⁻¹	2.8×10 ⁻¹	3.0	4.3×10 ⁻⁴	6.2

Table A. 4 Sensitivity Coefficients at [PAA]_o = 100 μM, [Fe(II)]_o = 25 μM, [ABTS]_o = 10 μM, t = 120 s

Rate Constant	Sensitivity Coefficient								Overall
	PAA	Fe(II)	Fe(IV)	ABTS ^{•+}	ABTS	CH ₃ CO ₂ [•]	CH ₃ COOO [•]	Fe(OH) ₃	
k _{1a}	12.1	60.0	79.5	51.2	59.3	79.8	392.0	2.3×10 ⁻¹	734.0
k _{1b}	13.2	68.5	74.9	55.9	65.4	81.7	450.0	2.6×10 ⁻²	809.5
k ₂	1.0×10 ⁻⁴	1.4×10 ⁻²	1.9×10 ⁻²	1.4×10 ⁻²	1.3×10 ⁻²	4.6×10 ⁻²	135.6	1.4×10 ⁻⁵	135.7
k ₃	9.1	52.1	85.0	28.5	32.7	46.7	259.0	5.8×10 ⁻²	513.0
k ₄	2.8	95.6	104.5	20.6	27.7	93.0	1472.0	1.8×10 ⁻²	1816.2
k ₅	9.4×10 ⁻⁵	1.8×10 ⁻³	6.2×10 ⁻³	3.1×10 ⁻⁴	2.7×10 ⁻⁴	1.7×10 ⁻³	753.4	1.0×10 ⁻⁶	753.5
k ₆	1.1×10 ⁻²	7.8×10 ⁻²	4.4×10 ⁻²	8.7×10 ⁻²	9.9×10 ⁻²	120	23.9	4.5×10 ⁻⁵	144.0
k ₇	2.0×10 ⁻¹	3.5	3.9	2.0	2.4	3.3	11.6	7.5×10 ⁻⁴	26.9
k ₈	8.9×10 ⁻³	3.2×10 ⁻²	1.9×10 ⁻²	3.8×10 ⁻²	4.3×10 ⁻²	13.3	171.5	6.4×10 ⁻⁵	184.8
k ₉	1.4×10 ⁻³	2.0×10 ⁻²	1.0×10 ⁻²	1.9×10 ⁻²	2.2×10 ⁻²	3.9×10 ⁻¹	897.6	6.8×10 ⁻⁶	898.0
k ₁₀	2.3×10 ⁻⁴	5.0	3.2	7.1	8.1	8.7	659.3	1.7×10 ⁻²	691.5
k ₁₁	2.8	7.8×10 ⁻⁴	1.5×10 ⁻³	1.4×10 ⁻³	1.5×10 ⁻³	6.0×10 ⁻²	3118.0	5.9×10 ⁻³	3121.0
k ₁₂	8.2×10 ⁻³	7.2×10 ⁻²	8.0×10 ⁻²	6.7×10 ⁻²	7.8×10 ⁻³	6.6×10 ⁻²	35.5	4.3×10 ⁻⁵	35.6
k ₁₃	10.7	45.5	35.0	23.4	27.0	34.9	68.5	8.2×10 ⁻⁴	245.0

Table A. 5 Sensitivity Coefficients at [PAA]_o = 100 μM, [Fe(II)]_o = 25 μM, [ABTS]_o = 5 μM, t = 2s

Rate Constant	Sensitivity Coefficient								Overall
	PAA	Fe(II)	Fe(IV)	ABTS ^{•+}	ABTS	CH ₃ CO ₂ [•]	CH ₃ COOO [•]	Fe(OH) ₃	
k _{1a}	4.3×10 ⁻²	2.8	3.0	1.1	1.6×10 ⁻¹	2.6	7.7	1.4×10 ⁻¹	17.5
k _{1b}	5.0×10 ⁻²	1.4	8.7×10 ⁻¹	1.3	1.8×10 ⁻⁴	1.5	2.4	4.0×10 ⁻²	7.50
k ₂	1.5×10 ⁻⁴	2.1×10 ⁻⁴	2.5×10 ⁻⁴	1.8×10 ⁻³	2.1×10 ⁻⁴	6.1×10 ⁻⁴	10.6	1.0×10 ⁻⁶	10.6
k ₃	4.5×10 ⁻²	3.4×10 ⁻¹	2.2	3.2×10 ⁻¹	3.7×10 ⁻²	2.9×10 ⁻¹	3.3×10 ⁻¹	2.4×10 ⁻²	3.50
k ₄	4.0×10 ⁻³	1.1	1.0	4.8×10 ⁻²	7.3×10 ⁻³	1.0	1.8	1.8×10 ⁻³	5.0
k ₅	1.4×10 ⁻¹⁰	5.3×10 ⁻¹⁰	9.6×10 ⁻⁹	1.3×10 ⁻⁵	1.0×10 ⁻⁹	7.5×10 ⁻¹⁰	2.6	1×10 ⁻¹⁰	2.6
k ₆	1.3×10 ⁻⁴	1.9×10 ⁻⁴	2.6×10 ⁻⁴	3.0×10 ⁻³	3.5×10 ⁻⁴	2.0	15.2	7.0×10 ⁻⁶	17.2
k ₇	1.7×10 ⁻³	2.1×10 ⁻²	1.0×10 ⁻²	1.2×10 ⁻²	1.7×10 ⁻³	1.9×10 ⁻²	6.0×10 ⁻¹	4.2×10 ⁻⁴	0.7
k ₈	3.5×10 ⁻⁶	1.5×10 ⁻⁵	4.5×10 ⁻⁵	1.2×10 ⁻⁴	1.7×10 ⁻⁵	2.1×10 ⁻⁵	4.5	2.0×10 ⁻⁶	4.5
k ₉	1.7×10 ⁻⁶	7.6×10 ⁻⁵	7.6×10 ⁻⁵	1.2×10 ⁻³	1.4×10 ⁻⁴	5.4×10 ⁻⁴	5.0×10 ⁻¹	9.7×10 ⁻⁷	0.5
k ₁₀	8.8×10 ⁻³	3.4×10 ⁻²	4.6×10 ⁻²	7.7×10 ⁻²	1.0×10 ⁻²	3.3×10 ⁻²	3.6×10 ⁻²	3.5×10 ⁻³	0.25
k ₁₁	2.3×10 ⁻⁵	8.7×10 ⁻⁵	8.3×10 ⁻⁵	6.2×10 ⁻⁵	9.0×10 ⁻⁶	8.4×10 ⁻⁵	3.5×10 ⁻¹	1.0×10 ⁻⁵	0.35
k ₁₂	1.1×10 ⁻⁴	1.8×10 ⁻³	1.7×10 ⁻³	1.3×10 ⁻³	4.4×10 ⁻⁵	1.7×10 ⁻³	2.5×10 ⁻¹	3.2×10 ⁻⁵	0.25
k ₁₃	5.2×10 ⁻²	3.0×10 ⁻¹	1.3×10 ⁻¹	1.6×10 ⁻¹	2.2×10 ⁻²	2.5×10 ⁻¹	2.1×10 ⁻¹	6.3×10 ⁻³	1.2

Table A. 6 Sensitivity Coefficients at [PAA]_o = 100 μM, [Fe(II)]_o = 25 μM, [ABTS]_o = 5 μM, t = 120s

Rate Constant	Sensitivity Coefficient								
	PAA	Fe(II)	Fe(IV)	ABTS ^{•+}	ABTS	CH ₃ CO ₂ [•]	CH ₃ COOO [•]	Fe(OH) ₃	Overall
k _{1a}	4.3×10 ³	1.5×10 ¹	2.6×10 ⁴	2.8×10 ¹	7.8×10 ¹	2.1×10 ⁴	2.2×10 ²	1.4×10 ¹	5.1×10 ⁴
k _{1b}	3.9×10 ³	1.8×10 ¹	1.0×10 ³	3.3×10 ¹	9.2×10 ¹	7.2×10 ²	6.0×10 ²	1.7×10 ¹	6.3×10 ³
k ₂	1.7×10 ²	4.1×10 ⁻³	5.8×10 ²	1.7×10 ⁻¹	3.2×10 ⁻¹	1.1×10 ¹	6.8×10 ¹	4.0×10 ⁻³	8.3×10 ²
k ₃	2.2×10 ²	5.4×10 ⁻¹	3.0×10 ²	5.6×10 ¹	9.3×10 ¹	3.7×10 ²	1.1×10 ³	5.1×10 ⁻¹	2.2×10 ³
k ₄	2.7×10 ²	1.4×10 ⁻¹	3.2×10 ²	2.9×10 ¹	1.2×10 ²	4.9×10 ²	2.1×10 ³	1.4×10 ⁻¹	3.3×10 ³
k ₅	7.5×10 ¹	7.5×10 ⁻⁵	1.4×10 ²	9.5×10 ⁻²	4.3×10 ⁻²	2.6×10 ²	1.5×10 ³	7.2×10 ⁻⁵	1.9×10 ³
k ₆	5.9×10 ¹	2.5	1.6×10 ¹	2.3	5.4	2.3×10 ²	1.3×10 ²	2.4	4.4×10 ²
k ₇	9.8×10 ¹	1.0	1.3×10 ²	9.5×10 ⁻¹	2.9	5.8×10 ²	2.1×10 ²	9.5×10 ⁻¹	1.0×10 ³
k ₈	1.5×10 ²	2.3×10 ⁻²	5.3×10 ¹	5.9×10 ⁻²	1.0	4.0×10 ⁵	1.2×10 ⁵	2.2×10 ⁻²	5.2×10 ⁵
k ₉	4.0	9.3×10 ⁻⁴	2.2×10 ²	4.6×10 ⁻²	5.7×10 ⁻²	1.8×10 ¹	1.7×10 ¹	8.8×10 ⁻⁴	2.6×10 ²
k ₁₀	1.2×10 ²	3.8	7.1×10 ³	6.0×10 ¹	8.8×10 ²	2.8×10 ²	8.3×10 ²	3.7	9.2×10 ³
k ₁₁	1.4×10 ¹	2.6×10 ⁻²	3.3×10 ²	4.8×10 ⁻²	2.9×10 ⁻²	1.8×10 ²	1.5×10 ¹	2.5×10 ⁻²	5.4×10 ²
k ₁₂	1.7×10 ²	7.6×10 ⁻¹	1.1×10 ²	1.6×10 ²	7.8×10 ⁻¹	1.7×10 ²	3.5×10 ¹	7.3×10 ⁻¹	6.4×10 ²
k ₁₃	6.5×10 ¹	5.7	1.3×10 ²	5.9	1.5×10 ¹	1.5×10 ³	1.1×10 ²	5.4	1.8×10 ³

REFERENCES

1. Anquandah GAK, Sharma VK, Panditi VR, Gardinali PR, Kim H, Oturan MA. Ferrate(VI) oxidation of propranolol: Kinetics and products. *Chemosphere*. 2013;91(1):105-109. doi:10.1016/j.chemosphere.2012.12.001
2. Qin Q, Chen X, Zhuang J. The fate and impact of pharmaceuticals and personal care products in agricultural soils irrigated with reclaimed water. *Crit Rev Environ Sci Technol*. 2015;45(13):1379-1408. doi:10.1080/10643389.2014.955628
3. Patel M, Kumar R, Kishor K, Mlsna T, Pittman CU, Mohan D. Pharmaceuticals of emerging concern in aquatic systems: Chemistry, occurrence, effects, and removal methods. *Chem Rev*. 2019;119(6):3510-3673. doi:10.1021/acs.chemrev.8b00299
4. Kim J, Zhang T, Liu W, Du P, Dobson JT, Huang CH. Advanced Oxidation Process with Peracetic Acid and Fe(II) for Contaminant Degradation. *Environ Sci Technol*. 2019;53(22):13312-13322. doi:10.1021/acs.est.9b02991
5. Huerta-Fontela M, Galceran MT, Ventura F. Occurrence and removal of pharmaceuticals and hormones through drinking water treatment. *Water Res*. 2011;45(3):1432-1442. doi:10.1016/j.watres.2010.10.036
6. Stackelberg PE, Furlong ET, Meyer MT, Zaugg SD, Henderson AK, Reissman DB. Persistence of pharmaceutical compounds and other organic wastewater contaminants in a conventional drinking-water-treatment plant. *Sci Total Environ*. 2004;329(1-3):99-113. doi:10.1016/j.scitotenv.2004.03.015

7. Stackelberg PE, Gibs J, Furlong ET, Meyer MT, Zaugg SD, Lippincott RL. Efficiency of conventional drinking-water-treatment processes in removal of pharmaceuticals and other organic compounds. *Sci Total Environ.* 2007;377(2-3):255-272. doi:10.1016/j.scitotenv.2007.01.095
8. Qian Y, Guo X, Zhang Y, et al. Perfluorooctanoic Acid Degradation Using UV-Persulfate Process: Modeling of the Degradation and Chlorate Formation. *Environ Sci Technol.* 2016;50(2):772-781. doi:10.1021/acs.est.5b03715
9. Zhang R, Sun P, Boyer TH, Zhao L, Huang CH. Degradation of pharmaceuticals and metabolite in synthetic human urine by UV, UV/H₂O₂, and UV/PDS. *Environ Sci Technol.* 2015;49(5):3056-3066. doi:10.1021/es504799n
10. Sun P, Lee WN, Zhang R, Huang CH. Degradation of DEET and caffeine under UV/Chlorine and simulated sunlight/Chlorine conditions. *Environ Sci Technol.* 2016;50(24):13265-13273. doi:10.1021/acs.est.6b02287
11. Gągól M, Przyjazny A, Boczkaj G. Wastewater treatment by means of advanced oxidation processes based on cavitation – A review. *Chem Eng J.* 2018;338(September 2017):599-627. doi:10.1016/j.cej.2018.01.049
12. Luo C, Sadhasivan M, Kim J, Sharma VK, Huang C-H. Revelation of Fe(V)/Fe(IV) Involvement in the Fe(VI)–ABTS System: Kinetic Modeling and Product Analysis. *Environ Sci Technol.* 2021;55(6):3976-3987. doi:10.1021/acs.est.0c07792
13. Kim J, Huang C-H. Reactivity of Peracetic Acid with Organic Compounds: A Critical Review. *ACS ES&T Water.* 2021;1(1):15-33.

doi:10.1021/acsestwater.0c00029

14. Ao X wei, Eloranta J, Huang CH, et al. Peracetic acid-based advanced oxidation processes for decontamination and disinfection of water: A review. *Water Res.* 2021;188. doi:10.1016/j.watres.2020.116479
15. Naota T, Takaya H, Murahashi SI. Ruthenium-catalyzed reactions for organic synthesis. *Chem Rev.* 1998;98(7):2599-2660. doi:10.1021/cr9403695
16. Rokhina E V., Makarova K, Golovina EA, Van As H, Virkutyte J. Free radical reaction pathway, thermochemistry of peracetic acid homolysis, and its application for phenol degradation: Spectroscopic study and quantum chemistry calculations. *Environ Sci Technol.* 2010;44(17):6815-6821. doi:10.1021/es1009136
17. Rothbart S, Ember EE, Van Eldik R. Mechanistic studies on the oxidative degradation of Orange II by peracetic acid catalyzed by simple manganese(ii) salts. Tuning the lifetime of the catalyst. *New J Chem.* 2012;36(3):732-748. doi:10.1039/c2nj20852k
18. Luukkonen T, Heyninck T, Rämö J, Lassi U. Comparison of organic peracids in wastewater treatment: Disinfection, oxidation and corrosion. *Water Res.* 2015;85:275-285. doi:10.1016/j.watres.2015.08.037
19. Zhang J, Zhu L, Shi Z, Gao Y. Rapid removal of organic pollutants by activation sulfite with ferrate. *Chemosphere.* 2017;186:576-579. doi:10.1016/j.chemosphere.2017.07.102

20. Shao B, Dong H, Sun B, Guan X. Role of Ferrate(IV) and Ferrate(V) in Activating Ferrate(VI) by Calcium Sulfito for Enhanced Oxidation of Organic Contaminants. *Environ Sci Technol.* 2019;53(2):894-902. doi:10.1021/acs.est.8b04990
21. Luo C, Feng M, Sharma VK, Huang CH. Oxidation of Pharmaceuticals by Ferrate(VI) in Hydrolyzed Urine: Effects of Major Inorganic Constituents. *Environ Sci Technol.* 2019;53(9):5272-5281. doi:10.1021/acs.est.9b00006
22. Lee Y, Kissner R, Von Gunten U. Reaction of ferrate(VI) with ABTS and self-decay of ferrate(VI): Kinetics and mechanisms. *Environ Sci Technol.* 2014;48(9):5154-5162. doi:10.1021/es500804g
23. Luo C, Feng M, Zhang T, Sharma VK, Huang C-H. Ferrate(VI) Oxidation of Pharmaceuticals in Hydrolyzed Urine: Enhancement by Creatinine and the Role of Fe(IV). *ACS ES&T Water.* 2021;(Vi). doi:10.1021/acsestwater.0c00255
24. Feng M, Cizmas L, Wang Z, Sharma VK. Activation of ferrate(VI) by ammonia in oxidation of flumequine: Kinetics, transformation products, and antibacterial activity assessment. *Chem Eng J.* 2017;323:584-591. doi:10.1016/j.cej.2017.04.123
25. Huang ZS, Wang L, Liu YL, et al. Impact of Phosphate on Ferrate Oxidation of Organic Compounds: An Underestimated Oxidant. *Environ Sci Technol.* 2018;52(23):13897-13907. doi:10.1021/acs.est.8b04655
26. Buffle MO, Schumacher J, Salhi E, Jekel M, von Gunten U. Measurement of the initial phase of ozone decomposition in water and wastewater by means of a continuous quench-flow system: Application to disinfection and pharmaceutical

- oxidation. *Water Res.* 2006;40(9):1884-1894. doi:10.1016/j.watres.2006.02.026
27. Vikesland PJ, Fiss EM, Wigginton KR, McNeill K, Arnold WA. Halogenation of bisphenol-A, triclosan, and phenols in chlorinated waters containing iodide. *Environ Sci Technol.* 2013;47(13):6764-6772. doi:10.1021/es304927j
28. Theil H. Economic forecasts and policy. *North-holl Publ Co.* 1961.
29. Esposito G, Frunzo L, Panico A, Pirozzi F. Model calibration and validation for OFMSW and sewage sludge co-digestion reactors. *Waste Manag.* 2011;31(12):2527-2535. doi:10.1016/j.wasman.2011.07.024
30. Zhang T, Huang CH. Modeling the Kinetics of UV/Peracetic Acid Advanced Oxidation Process. *Environ Sci Technol.* 2020;54(12):7579-7590. doi:10.1021/acs.est.9b06826
31. Chateauneuf J, Luszyk J, Ingold KU. Spectroscopic and kinetic characteristics of aroyloxy radicals. 2. Benzoyloxy and ring-substituted aroyloxy radicals. *J Am Chem Soc.* 1988;110(9):2886-2893. doi:10.1021/ja00217a032
32. Scott SL, Chen W, Bakac A, Espenson JH. 2,2'-Azinotf. 1993;(3):6710-6714.
33. Piesiak A, Schuchmann MN, Zegota H, Clemens von S. β -Hydroxyethylperoxy Radicals: A Study of the γ -Radiolysis and Pulse Radiolysis of Ethylene in Oxygenated Aqueous Solutions. *Zeitschrift fur Naturforsch - Sect B J Chem Sci.* 1984;39(9):1262-1267. doi:10.1515/znb-1984-0920
34. Lu Z, Continetti RE. Dynamics of the acetyloxy radical studied by dissociative

- photodetachment of the acetate anion. *J Phys Chem A*. 2004;108(45):9962-9969.
doi:10.1021/jp040355v
35. Audenaert WTM, Callewaert M, Nopens I, et al. Full-scale modelling of an ozone reactor for drinking water treatment. *Chem Eng J*. 2010;157(2-3):551-557.
doi:10.1016/j.cej.2009.12.051
36. Xianmin Z. New method with high confidence for validation of computer simulation models of flight systems. *J Syst Eng Electron*. 1993;4(4):43-52.
37. Sharma VK, Zboril R, Varma RS. Ferrates: Greener oxidants with multimodal action in water treatment technologies. *Acc Chem Res*. 2015;48(2):182-191.
doi:10.1021/ar5004219
38. Rush JD, Zhao Z, Bielski BHJ. Reaction of ferrate(VI)/ferrate(V) with hydrogen peroxide and superoxide anion - A stopped-flow and premix pulse radiolysis study. *Free Radic Res*. 1996;24(3):187-198. doi:10.3109/10715769609088016
39. Melton JD, Bielski BHJ. Studies of the kinetic, spectral and chemical properties of Fe(IV) pyrophosphate by pulse radiolysis. *Int J Radiat Appl Instrumentation Part*. 1990;36(6):725-733. doi:10.1016/1359-0197(90)90169-I
40. Løgager T, Holcman J, Sehested K, Pedersen T. Oxidation of Ferrous Ions by Ozone in Acidic Solutions. *Inorg Chem*. 1992;31(17):3523-3529.
doi:10.1021/ic00043a009
41. Sharma VK, Bielski BHJ. Reactivity of Ferrate(VI) and Ferrate(V) with Amino

Acids. *Inorg Chem.* 1991;30(23):4306-4310. doi:10.1021/ic00023a005

42. Pestovsky O, Bakac A. Aqueous ferryl(IV) ion: Kinetics of oxygen atom transfer to substrates and oxo exchange with solvent water. *Inorg Chem.* 2006;45(2):814-820. doi:10.1021/ic051868z
43. Rush JD, Bielski BHJ. of Ferrate(V) in Neutral. 1994;(V):200-203.
44. Rush JD, Bielski BHJ. Kinetics of Ferrate(V) Decay in Aqueous Solution: A Pulse-Radiolysis Study. *Inorg Chem.* 1989;28(21):3947-3951. doi:10.1021/ic00320a004
45. Luo C, Feng M, Sharma VK, Huang CH. Revelation of ferrate(VI) unimolecular decay under alkaline conditions: Investigation of involvement of Fe(IV) and Fe(V) species. *Chem Eng J.* 2020;388(October 2019):124134. doi:10.1016/j.cej.2020.124134